

Modelling flood levels associated with ice consolidation events triggered by upstream ice jam release waves in the Hay River Delta, NWT

by

Michael De Coste

A thesis submitted in partial fulfillment of the requirements for the degree of

Master of Science

In

Water Resources Engineering

Department of Civil and Environmental Engineering
University of Alberta

© Michael De Coste, 2017

Abstract

The Town of Hay River, located in the North West Territories, Canada, is vulnerable to ice jam flooding occurring in the adjacent Hay River delta. The most extreme flooding events have occurred when ice jams in the channels of the delta were pushed downstream towards the mouth of Great Slave Lake. This movement has been linked to incoming waves from ice jam release events in the upstream reaches of the Hay River. The objective of this study was to incorporate the effect of an upstream ice jam release wave into the prediction of ice jam caused flood levels in the delta. This was achieved by integrating the capabilities of a series of one-dimensional (1-D) models, including the *River1D* Ice Jam Release model, the *River1D* Network model, and HEC-RAS. The method was validated with breakup events from 2008 and 2009. It was then used to simulate a large number of scenarios encompassing various combinations of ice and water conditions in the upper reach and the delta of the Hay River. Multiple linear regression analyses were then applied to the model results to facilitate the development of a flood level prediction tool to assess ice jam flood risk for the use of the Town of Hay River.

Acknowledgments

The author would like to extend his thanks to his supervisor, Dr. Yuntong She, for her constant guidance and support throughout this project, which is deeply appreciated. Thank you as well to Dr. Mark Loewen and Dr. Wei Liu for being a part of the examining committee.

Thanks are also extended to the University of Alberta's River Ice Research Group, in particular Dr. Faye Hicks and Julia Blackburn for their assistance and guidance.

This research was funded through a grant from the Natural Sciences and Engineering Research Council of Canada which is gratefully acknowledged.

The author would also like to extend thanks to his family and friends for their guidance and support throughout this research.

Table of Contents

Chapter 1 : Introduction	1
1.1 Background	1
1.2 Previous Research	2
1.3 Study Objectives	5
Chapter 2 : Methodology.....	11
2.1 Study Reach Description.....	11
2.2 Model Description and Setup.....	11
2.2.1 River1D Ice Jam Release Model	11
2.2.2 <i>River1D</i> Network Model	15
2.2.3 HEC-RAS	18
2.3 Integrated Modelling Method.....	19
2.4 Modelling Domain	20
Chapter 3 : Calibration and Validation.....	26
3.1 Validation of <i>River1D</i> Network Model.....	26
3.2 Breakup Modelling.....	27
3.2.1 2008 Breakup.....	28
3.2.2 2009 Breakup.....	30
Chapter 4 : Model Application	43
4.1 Hypothetical Scenarios.....	43

4.2 Multiple Linear Regression (MLR) Analyses	48
4.3 Flood Level Prediction Tool	57
Chapter 5 : Summary and Conclusions	71
References	73
Appendix A: Matlab Code of the Flood Level Prediction Tool	76

List of Tables

Table 3.1 Comparison of modelled flow splits to 2007 ADCP measurements.	27
Table 4.1 List of documented historical ice jam events in the upstream reaches of the Hay River.	45
Table 4.2 List of documented historical ice jams in the Hay River Delta.	47
Table 4.3 Selected values of key variables in the simulated hypothetical events.....	48
Table 4.4 List of MLR equations for each location in the East Channel of the Hay River Delta.	50
Table 4.5 Rankings of the five key variables.....	53
Table 4.6 Range of modelled top of ice elevations at key locations in the East Channel of the Hay River Delta.	54
Table 4.7 List of ranked MLR equations in the East Channel of the Hay River Delta.	55

List of Figures

Figure 1.1 Map of the Hay River Basin (Adapted from Watson (2011)).	7
Figure 1.2 Map of the Hay River Delta (adapted from Brayall and Hicks (2012)). Numbers along the channel indicate river kilometers from the source.	8
Figure 1.3 2008 Ice Jam Flood in the East Channel of the Hay River Delta (University of Alberta River Ice Research Group).	9
Figure 1.4 2008 Ice Jam Flooding in the Old Town District of the Town of Hay River (University of Alberta River Ice Research Group).	10
Figure 2.1 Bed profile of equivalent rectangular channel for the Hay River showing key landmarks and gauge stations (Adapted from Hicks et al., 1992).	22
Figure 2.2 Open channel junction configurations for (a) combing junction and (b) dividing junction (adapted from Shabayek 2002).	23
Figure 2.3 Flowchart of integrated modelling method.	24
Figure 2.4 Plan view schematic of River1D Network model geometry of Hay River Delta.	25
Figure 3.1 Locations of ADCP cross sections in the Hay River Delta (Brayall 2011).	33
Figure 3.2 Comparison of flow apportionment into East Channel between River1D Network model and River2D (Brayall and Hicks, 2012).	34
Figure 3.3 Example aerial photo of ice jam in the East Channel of the Hay River Delta taken May 5, 2008 (Brayall 2011).	35

Figure 3.4 Calibration of 2008 upstream ice jam using data from WSC Hay River near Hay River and EMO gauge at Pine Point Bridge.	36
Figure 3.5 Ice Jam Map for modelled 2008 release (adapted from Hicks et al., 1992).....	36
Figure 3.6 Ice jam release hydrograph for the 2008 release event modelled with the River1D Network model.....	37
Figure 3.7 Pre a) and post b) wave delta ice jam configurations for East Channel-2008.....	38
Figure 3.8 Pre a) and post b) wave delta ice jam configurations for West Channel-2008.	39
Figure 3.9 Ice Jam Map for modelled 2009 release (adapted from Hicks et al., 1992).....	40
Figure 3.10 Ice jam release hydrograph for the 2009 release event modelled with the River1D Network model.....	40
Figure 3.11 Pre (a) and post b) wave delta ice jam configurations for East Channel-2009.	41
Figure 3.12 Pre (a) and post b) wave delta ice jam configurations for West Channel-2009.....	42
Figure 4.1 Comparison between the predicted and the simulated top of ice level at Km 1108.3 for the two regression methods: a) without rank and b) with rank.	59
Figure 4.2 Comparison between the predicted and the simulated top of ice level at Km 1109 for the two regression methods: a) without rank and b) with rank.	60
Figure 4.3 Comparison between the predicted and the simulated top of ice level at Km 1109.5 for the two regression methods: a) without rank and b) with rank.	61

Figure 4.4 Comparison between the predicted and the simulated top of ice level at Km 1109.98 for the two regression methods: a) without rank and b) with rank.	62
Figure 4.5 Comparison between the predicted and the simulated top of ice level at Km 1111 for the two regression methods: a) without rank and b) with rank.	63
Figure 4.6 Comparison between the predicted and the simulated top of ice level at Km 1111.55 for the two regression methods: a) without rank and b) with rank.	64
Figure 4.7 Comparison between the predicted and the simulated top of ice level at Km 1112.2 for the two regression methods: a) without rank and b) with rank.	65
Figure 4.8 Comparison between the predicted and the simulated top of ice level at Km 1112.4 for the two regression methods: a) without rank and b) with rank.	66
Figure 4.9 Comparison between the predicted and the simulated top of ice level at Km 1113.22 for the two regression methods: a) without rank and b) with rank.	67
Figure 4.10 Comparison between the predicted and the simulated top of ice level at Km 1113.61 for the two regression methods: a) without rank and b) with rank.	68
Figure 4.11 Comparison of the top of ice level predicted by the proposed tool, the IJPG and the observation for the 1992 flooding event.	69
Figure 4.12 Comparison of the top of ice level predicted by the proposed tool, the IJPG and the key landmarks for the 2007 flooding event.....	70

List of Symbols

A = the total area of the cross-section under the water surface (m^2)

A_w = cross-sectional area of the water, perpendicular to the flow (m^2)

a_1 = velocity weighing coefficient of the main channel (*dimensionless*)

a_2 = velocity weighing coefficient of the lateral channel (*dimensionless*)

a_j ($j = 1, 6$) = regression coefficients (*dimensionless*)

B = width of the ice accumulation (m)

b_j ($j = 1, 6$) = ranked regression coefficients (*dimensionless*)

C_f = cohesion (Pa)

C_* = the nondimensional Chezy's coefficient (*dimensionless*)

e = porosity of the ice accumulation (*dimensionless*)

g = acceleration due to gravity (m^2/s)

H = the depth of flow under the water surface (m)

H_w = depth of water flow (m)

h_e = energy head loss (m)

K_x = a passive pressure coefficient (*dimensionless*)

L_j = length of the upstream jam (km)

LL = lake level (m)

L_1 = the length of the main channel control volume (m)

L_2 = the length of the lateral channel control volume (m)

n = Manning's resistance coefficients of the channel bed (*dimensionless*)

Q = the total discharge, including both water and ice flow (m^3/s)

Q_c = carrier discharge of upstream jam (m^3/s)

Q_w = water discharge (m^3/s)

R = hydraulic radius (m)

S = stream slope (*dimensionless*)

SC = the total rank of the scenario predicted by the multiple linear regression equation (*dimensionless*)

S_f = friction slope determined using Manning's equation (*dimensionless*)

S_L = the rank for the length of the upstream jam (*dimensionless*)

S_Q = the rank for carrier discharge (*dimensionless*)

S_S = the rank for toe shift of the delta jam (*dimensionless*)

S_T = the rank for the toe location of the upstream jam (*dimensionless*)

S_{WL} = the rank for the lake level (*dimensionless*)

S_o = river bed slope (*dimensionless*)

TOI = simulated top of ice levels in the delta region (m)

TS = toe shift of the delta jam (km)

Tj = toe location of upstream jam (km)

t_i = thickness of the ice jam accumulation (m)

V = ice and water velocity (m/s)

V_w = velocity of water flow (m/s)

V_1 = average velocity of main channel (m/s)

V_2 = average velocities of lateral channel (m/s)

x = longitudinal co-ordinate (m)

Y_1 = depth of water at the cross section of lateral channel (m)

Y_2 = depth of water at the cross section of main channel (m)

Z_1 = elevation of the main channel invert (m)

Z_2 = elevation of the lateral channel invert (m)

ρ = density of water (kg/m^3)

ρ_i = density of ice (kg/m^3)

τ = shear stress of flow on underside of accumulation (Pa)

λ_1 = an empirically determined coefficient approximating bank resistance effects on the ice run
(*dimensionless*)

λ_2 = an empirical coefficient accounting for the longitudinal dispersion of the released ice mass
(*dimensionless*)

ϕ = angle of internal friction of the ice accumulation ($^\circ$)

$\xi = Q_{WB}/Q_{WA}$ is a discharge ratio;

List of Abbreviations

AB=Alberta

ADCP=Acoustic Doppler Current Profiler

BC=British Columbia

CDG=Characteristic-Dissipative-Galerkin

EMO=Emergency Measures Organization

IJPG=Ice Jam Profile Generator

MLR=Multiple Linear Regression

NWT=North West Territories

TOI=Top of Ice

WSC=Water survey of Canada

U of A=University of Alberta

Chapter 1 : Introduction

1.1 Background

Dynamic breakup is a critical event in many northern rivers. High flows resulting from spring snowmelt runoff lift an existing ice cover out of place, break it, and carry it downstream. An ice jam can form when this broken ice becomes blocked in the channel upon entering constrictions or flowing into intact ice cover. Flooding often results from significant flow obstructions or from the release of ice jams creating waves of water and ice. Ice jam caused flooding can occur incredibly fast, potentially leaving nearby communities with little notice and creating challenges in accurately predicting both the severity and timing of such events.

The Hay River originates in British Columbia (BC) and flowing through northern Alberta (AB) into the North West Territories (NWT), as shown in Figure 1.1. Due to its north flowing nature and a steep reach containing two waterfalls, dynamic breakup occurs almost yearly. The general pattern of breakup progression has been found to be relatively consistent from year to year (Kovachis et al., 2010). Breakup begins with melting in the headwaters of the southern portion of the basin. This snowmelt runoff lifts and break the ice cover, carrying it downstream to create a series of ice jams throughout the upstream reaches of the river. These ice jams can release sending a wave traveling downstream towards the Hay River Delta, where the Town of Hay River is located.

The entrance of the Hay River Delta is known as the Forks (km 1108), a location where the Hay River splits into the East Channel and the West Channel. These channels flow around Vale Island, the location of the Old Town district. The “New Town,” located upstream of the delta in an area less prone to flooding, was established after a particularly severe flood that

occurred in 1963. The delta region is also home to several fishing villages, including the West Point Fishing Village on the east side of the West Channel, as well as the Katl'odeeche First Nations Reserve on the east side of the East Channel. Figure 1.2 shows a detailed map of the Hay River delta.

At the onset of breakup, small ice accumulations form within the delta. The arrival of the upstream ice jam release waves causes great increase in discharge and brings large amount of additional ice. Thus, the small accumulations within the delta consolidate, becoming much longer and thicker ice jams. The arrival of the wave also pushes the toe of the delta jams downstream towards the mouth of the river, which has been witnessed in 1965, 1978, 1985, 1989, 1992, and 2007. In these instances, flooding resulted on Vale Island. In 2008, severe flooding occurred in the Hay River Delta when an ice jam in the East Channel was pushed further downstream by an incoming release wave. Figure 1.3 shows this flood in the upstream region of the East Channel and Figure 1.4 shows the extent of the flooding in the Old Town district. This flood resulted in the declaration of a state of emergency for the Town of Hay River and over one million dollars in damages. Minor flooding has also occurred in 2009 and 2010 as a result of ice jam shifting in the delta. Therefore, the direct effects of ice jam release waves on the conditions of ice jams in the delta are a vital component of developing a flood evacuation plan for the community.

1.2 Previous Research

Studies have been focusing on predicting ice jam caused flooding in the Hay River Delta through computer modelling. Gerard and Stanley (1988) developed a first generation flood forecast procedure based around historical flow data. This procedure was limited by the

unpredictable nature of jam shifting in the delta and the difficulty in estimating the timing and magnitude of ice jam release waves from upstream. Gerard and Jasek (1989) further evaluated this procedure, recommending flood mitigation techniques for the West Channel, additional measurements in the East Channel, and adaptation of the model developed into a computer based format. Gerard et al. (1990) utilised unsteady flow analysis to evaluate flow waves caused by upstream ice jam releases. The models ability to capture wave travel times and peak discharges was limited, due to a lack of field data on flood surges in the Hay River to use in refining the model's equations. Hicks et al. (1992) modelled ice jam release waves on the Hay River using the *cdg1-D* model (the precursor to *RiverID*), and the resulting peak flows at the delta were used together with the *ICEJAM* model (Flato and Gerard, 1986) to estimate expected ice jam flood levels in the Town. At that time, no data was available on ice jam release events on the Hay River, so the initial ice jam profiles were estimated using an equilibrium ice jam approximation to estimate worst-case scenarios, and a suite of hypothetical ice jam release events were modeled to give a range of possible outcomes.

She and Hicks (2005) later enhanced the *cdg1-D* model to add the calculation of actual ice jam profiles for release, based on the same algorithm used in the *ICEJAM* model, calling it the *RiverID* model. Watson (2011) applied this updated model to multiple ice jam release events documented on the Hay River from the monitoring program during the years 2007-2009. The monitoring program consisted of remote water level monitoring at four sites along the Hay River, as well as time lapse cameras and aerial reconnaissance flights. This enabled a detailed overview and timeline of the breakup progress of these years, with observations of the movement of waves through the Hay River obtained. It was found that the model accurately reproduced the

timing and severity of the release wave in comparison to measurements taken at stations along the Hay River.

Brayall and Hicks (2012) utilised the University of Alberta's (U of A) two-dimensional (2-D) numerical model *River2D* to simulate the flood levels resulting from ice jam consolidation events caused by incoming waves. This study involved the use of a summer survey to obtain the bathymetry of the Hay River Delta, as well as observations taken during both freeze up and breakup to better understand winter conditions and verify the accuracy of the model in depicting the breakup events. 11 ice jam profiles were modelled. The model results were used to develop an 'ice jam profile generator' (IJPG) to predict the expected flood levels at key locations in the town, using peak discharge estimates from the *River1D* model as input. Although this dual-model flood forecasting system is effective for predicting expected ice jam flood levels, it has three key limitations. First, the 2-D modelling process was considered time and labor intensive, making it difficult to apply to other sites. The transverse variations within individual channels provided by the 2-D model are not the highest concern in flood forecasting. Second, the resulting profile generator does not explicitly include movement of the ice jam toe in the delta during consolidation events, but instead relies on the 'typical' locations of these ice jam toes in the past. Third, the IJPG assumes that all incoming ice jam release waves to the Town will cause an ice jam consolidation (shoving) event; however, this does not always happen.

Zhao (2011) demonstrated the potential of using fuzzy logic and artificial neural networks to forecast breakup timing and severity for the Town of Hay River. A system of input variables was identified for these systems with both long and short lead times, including accumulated degree days of freezing and thawing, ice thickness, water levels on the days of freeze up onset and onset of water rise, accumulated rainfall and snowfall, and peak discharge.

The study also showed that the peak discharge caused by an upstream ice jam release event was an important factor affecting the ice jam flood severity in the delta.

1.3 Study Objectives

This study consisted of two objectives: (1) to incorporate the effects of upstream ice jam release waves in the prediction of ice jam flood levels within the Hay River Delta and explicitly include the effect of jam toe shifting during consolidation events, and (2) to investigate the possibility of using 1-D network modelling to provide an operational tool for flood forecasting. To achieve these objectives three separate models were applied sequentially and iteratively: (1) the updated University of Alberta's *RiverID* Ice Jam Release model (She and Hicks, 2006), which includes consideration of ice effects, was used for simulating the ice jam release events, (2) the new University of Alberta's *RiverID* Network model (Blackburn et al., 2015) was used for simulating wave propagation in the multi-channel network, and (3) the US Army Corps of Engineers *HEC-RAS* model was used for simulating the ice jam profiles within the individual delta channels. Data previously gathered from the extensive field program in the Hay River region was used to calibrate and validate the new integrated modelling method. The validated method was then utilised to simulate a series hypothetical scenarios and the results were used in the development of a flood level prediction tool.

This thesis details how the objectives of this study were achieved. Chapter 2 describes the study reach, the utilised hydrodynamic models, and the integrated modelling method. Chapter 3 describes the validation of the proposed method. Chapter 4 then discusses the large set of hypothetical modelling scenarios that the methodology was applied to. The rationale behind the selection of these scenarios is also detailed. Following this, the methods of statistical analysis

used in interpreting the obtained data are summarized, with the description of the final flood level prediction tool and its validation then detailed.

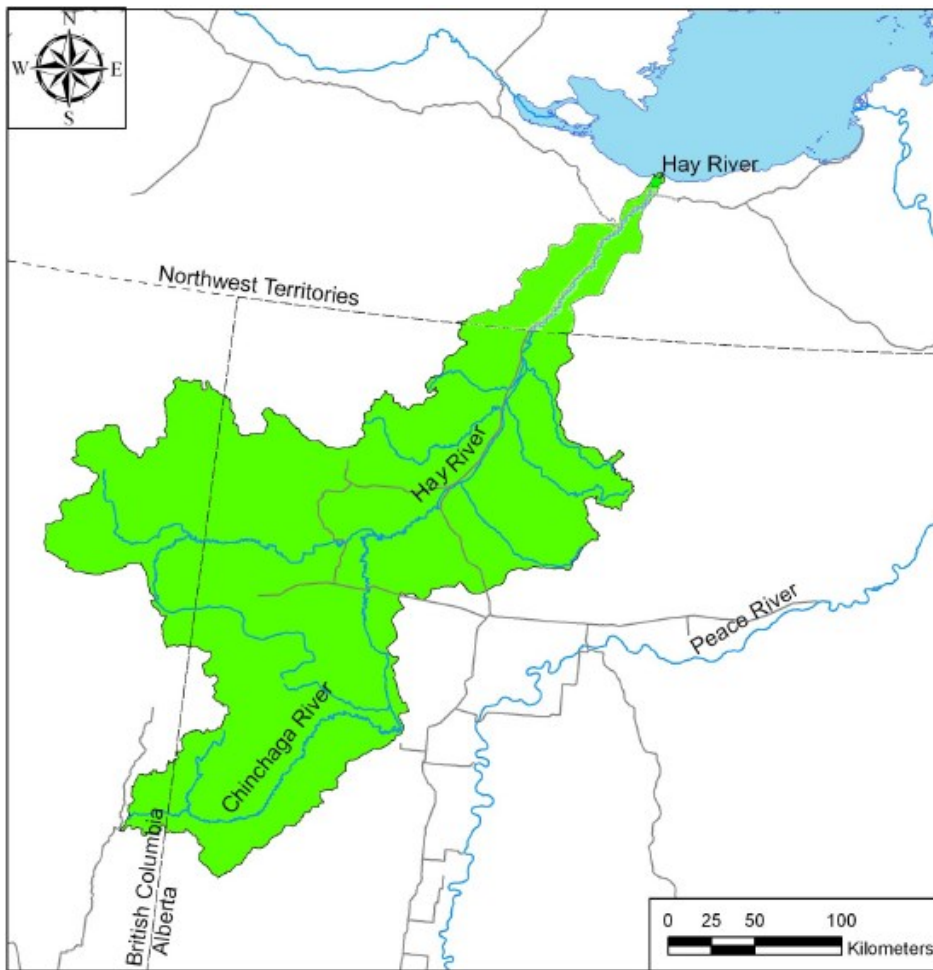


Figure 1.1 Map of the Hay River Basin (Adapted from Watson (2011)).

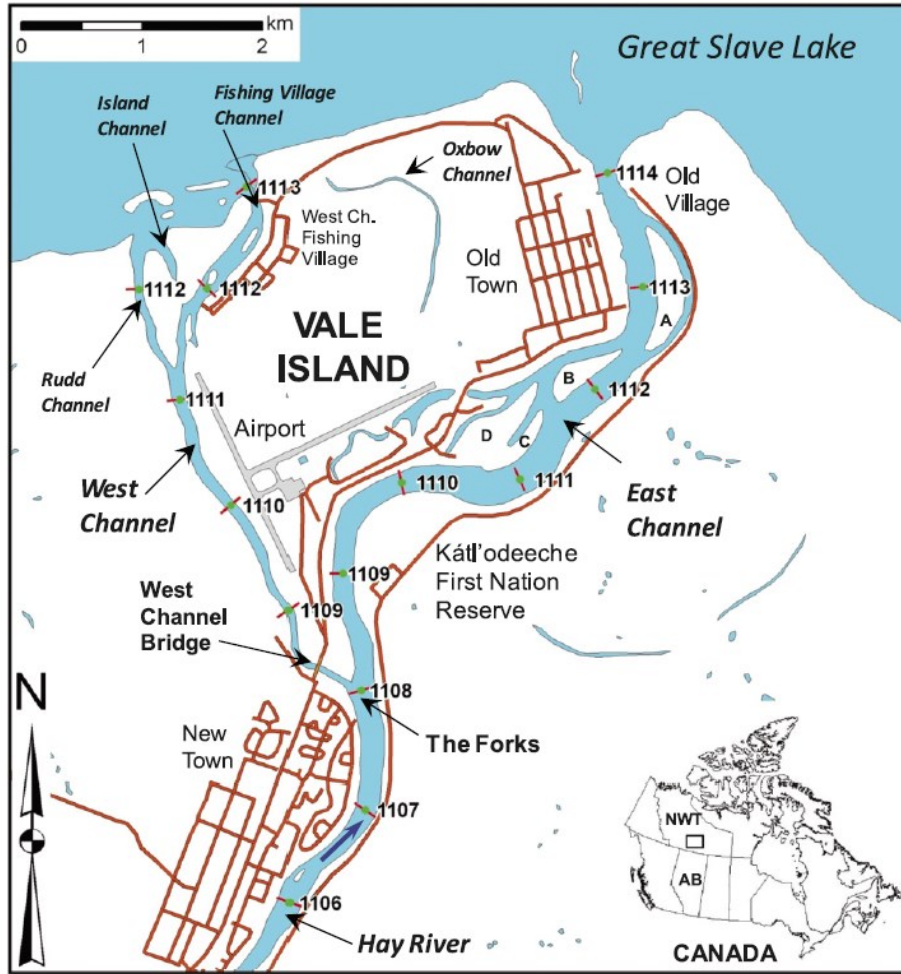


Figure 1.2 Map of the Hay River Delta (adapted from Brayall and Hicks (2012)). Numbers along the channel indicate river kilometers from the source.



Figure 1.3 2008 Ice Jam Flood in the East Channel of the Hay River Delta (University of Alberta River Ice Research Group).



Figure 1.4 2008 Ice Jam Flooding in the Old Town District of the Town of Hay River
(University of Alberta River Ice Research Group).

Chapter 2 : Methodology

2.1 Study Reach Description

The relevant reach of the Hay River extends from the boundary between the NWT and AB border at river station km 945.17 to Great Slave Lake at km 1114.24. The bed profile of this reach was previously determined by Gerard et al., 1990 and Hicks et al., 1992, averaged within five sub-reaches (Figure 2.1). River stations were measured from the origin of the river. The upper part of the study reach is relatively flat with an average slope of 0.0002. The region between km 1034 to km 1048 includes the Alexandra Falls (km 1034), the Louise Falls (km 1037.1), and a very steep gorge section. The average slope is 0.0058. Downstream of km 1048 extending to the entrance of the delta at km 1108, the bank height gradually decreases and the slope of the river reduces to an average of 0.0005. Ice jams frequently form in this region and their releases have been linked to severe delta flooding (Gerard and Stanley, 1988). At km 1108, the river splits and forms the delta with an average slope of 0.0001. The gauge stations used for calibration or as boundary conditions in this study are also shown, including the Water Survey of Canada (WSC) gauges of Hay River near NWT/AB border (km 945.5), near Hay River (km 1095) and at Great Slave Lake (km 1114.24), as well as the Emergency Measures Organization (EMO) at Alexandra Fall (km 1035) and Pine Point Bridge (km 1098).

2.2 Model Description and Setup

2.2.1 *RiverID* Ice Jam Release Model

The first component of the proposed modelling method utilised in this research is the *RiverID* Ice Jam Release model (She and Hicks, 2006). This model was built upon the public domain *RiverID* software employing a characteristic-dissipative-Galerkin (CDG) finite element scheme (Hicks and Steffler, 1992). It is capable of simulating unimpeded ice jam release wave

propagation in a single channel. The ice effects are simplified by considering the ice as a portion of the water, assuming ice and water move together at the same velocity. The conservation equations of total mass and momentum of ice and water take the same form as the St. Venant equations for open channel flow with the addition of a term accounting for ice resistance at the bank interfaces. For rectangular channels, the conservation of total mass and momentum equations can be written as:

$$\frac{\partial A}{\partial t} + \frac{\partial Q}{\partial x} = 0 \quad (2-1)$$

$$\frac{\partial Q}{\partial t} + \frac{\partial(VQ)}{\partial x} + gA \frac{\partial H}{\partial x} = gA(S_o - S_f) - 2\lambda_1 g B t_i S_f \quad (2-2)$$

where

Q = the total discharge, including both water and ice flow (m^3/s);

H = the depth of flow under the water surface (m);

A = the total area of the cross-section under the water surface (m^2);

λ_1 = an empirically determined coefficient approximating bank resistance effects on the ice run (*dimensionless*);

V = ice and water velocity (m/s);

S_o = river bed slope (*dimensionless*);

B = width of the accumulation (m);

t_i = thickness of the ice jam accumulation (m);

S_f = friction slope determined using Manning's equation (*dimensionless*):

$$S_f = \frac{n^2 V |V|}{R^{4/3}} \quad (2-3)$$

n = Manning's resistance coefficients of the channel bed (*dimensionless*);

R = hydraulic radius (*m*);

Equations (2-1) and (2-2) are solved in an uncoupled sequence with the ice mass continuity equation:

$$\frac{\partial t_i}{\partial t} + \frac{\partial (V t_i)}{\partial x} + \frac{V t_i}{B} \frac{dB}{dx} = \lambda_2 \frac{\partial^2 t_i}{\partial x^2} \quad (2-4)$$

where λ_2 is another empirical coefficient accounting for the longitudinal dispersion of the released ice mass. This parameter, together with λ_1 , is used to empirically approximate the full ice dynamics.

To make it convenient to simulate ice jam release events, the ice jam stability equation (Pariset et al., 1966; Uzuner and Kennedy, 1976) was also incorporated into the model to calculate the initial steady state ice jam profile prior to release.

$$t_i \frac{\partial t_i}{\partial x} = a + b t_i + c t_i^2 \quad (2-5)$$

in which:

$$a = \frac{\tau}{2K_x \gamma_e} \quad (2-6)$$

$$b = \frac{g \rho_i S - \left(\frac{2C_f}{B} \right)}{2K_x \gamma_e} \quad (2-7)$$

$$c = \frac{-C_o}{K_x B} \quad (2-8)$$

$$\gamma_e = \frac{g \rho_i}{2} (1 - e) \left(1 - \frac{\rho_i}{\rho}\right) \quad (2-9)$$

Where:

t_i = thickness of the ice jam accumulation (m);

x = longitudinal co-ordinate (m);

τ = shear stress of flow on underside of accumulation (Pa);

K_x = a passive pressure coefficient (*dimensionless*);

g = acceleration due to gravity (m^2/s);

ρ_i = density of ice (kg/m^3);

S = stream slope (*dimensionless*);

C_f = cohesion (Pa);

ϕ = angle of internal friction of the ice accumulation ($^\circ$);

$C_o = \tan \phi$

e = porosity of the ice accumulation (*dimensionless*);

ρ = density of water (kg/m^3);

In the *River1D* model, the jam stability equation is solved in a decoupled way with the unsteady flow hydrodynamic equations. Specifically, an initial ice jam profile is first assumed. The unsteady flow hydrodynamic equations are then run with the imposed ice thickness until a

steady state is reached. Based on the new steady state solution, a new ice jam profile is calculated. These steps are repeated until the change in the computed ice jam profile and hydrodynamic condition is within a specified tolerance.

2.2.2 *River1D* Network Model

The second model utilised in the proposed method is the *River1D* Network model, also built upon the *River1D* software. It models wave propagation in channel networks under both open water and intact (non-moving) ice cover conditions. It does not assume equal energy or equal water levels at the junction, as is the case in many other 1-D network models. The model accounts for significant physical effects at junctions such as gravity forces and channel resistance which are critical for modelling dynamic wave propagation. These effects are particularly important in river deltas due to the largeness of horizontal scale relative to the vertical scale (Blackburn et al., 2015). Therefore, the model is essential for this study, as the capability to model highly dynamic ice jam release waves through the Hay River Delta is required.

In open channel networks, the individual channel reaches are connected through junctions. The Network model solves the conservation of mass and momentum equations in both single channels and at the junctions. In rectangular single channels, the 1-D conservation of mass and momentum takes the form of the St. Venant equations:

$$\frac{\partial A_w}{\partial t} + \frac{\partial Q_w}{\partial x} = 0 \quad (2-10)$$

$$\frac{\partial Q_w}{\partial t} + \frac{\partial (V_w Q_w)}{\partial x} + g A_w \frac{\partial H_w}{\partial x} = g A_w (S_o - S_f) \quad (2-11)$$

where:

A_w = cross-sectional area of the water, perpendicular to the flow (m^2);

H_w = depth of water flow (m);

Q_w = water discharge (m^3/s);

V_w = velocity of water flow (m^2/s);

All other variables are as previously defined.

The equations at the junctions are based on the theoretical study conducted by Shabayek (2002). These junctions consist of three individual channels, arranged in configurations which are considered combining or dividing. Rectangular channel geometry is considered and the layouts of these junctions are illustrated in Figure 2.2. In a combining junction (Figure 2.2a), subscript A and C indicate the sections in the main channel just upstream and downstream of the junction, while subscript B indicates the section of the lateral channel just upstream of the junction. The flow variables to be evaluated are the water depth and discharge at these three sections. Two control volumes, one for the main channel and one for the lateral channel, are considered and each has a conservation of momentum equation (Shabayek, 2002). For the main channel control volume:

$$-\rho Q_{WC} V_{WC} + \rho Q_{WC} V_{WA} = \frac{\gamma H_{WC}^2}{2} B_C - \frac{\gamma H_{WA}^2}{2} B_A (1 - \xi) + \frac{\gamma}{2} \left(\frac{H_{WC} + H_{WB}}{2} \right)^2 (B_A (1 - \xi) - B_C) + \gamma \left(\frac{H_{WC} B_C + H_{WA} B_A (1 - \xi)}{2} \right) L_1 S_o - \rho \left(\frac{V_{WA}^2}{C_*} \right) (B_A (1 - \xi) + y_A) L_1 \quad (2-12)$$

and for the lateral channel control volume:

$$-\rho Q_{WB} V_{WB} + \rho Q_{WB} V_{WA} = \frac{\gamma H_{WB}^2}{2} B_B - \frac{\gamma H_{WA}^2}{2} B_A \xi + \frac{\gamma}{2} \left(\frac{H_{WC} + H_{WB}}{2} \right)^2 (B_A \xi - B_B) + \gamma \left(\frac{H_{WB} B_B + H_{WA} B_A \xi}{2} \right) L_2 S_o - \rho \left(\frac{V_{WA}^2}{C_*} \right) (B_A \xi + y_A) L_2 \quad (2-13)$$

where:

$\xi = Q_{WB}/Q_{WA}$ is a discharge ratio;

L_1 = the length of the main channel control volume (m);

L_2 = the length of the lateral channel control volume (m);

C^* = the nondimensional Chezy's coefficient;

With the other variables as defined in Figure 2.2a. The interfacial shear force, the separation zone shear force, and the centrifugal effects which were accounted for in Shabayek (2002)'s theoretical model are neglected in the current version of the model.

In a dividing junction (Figure 2.2b), subscript C and A indicate the sections in the main channel just upstream and downstream of the junction, while subscript B indicates the section of the lateral channel just downstream of the junction. Similarly, two control volumes, one for the main channel and one for the lateral channel, are considered and each has a conservation of momentum equation (Shabayek, 2002). For the main channel control volume:

$$\rho Q_{WC} V_{WC} - \rho Q_{WC} V_{WA} = \frac{\gamma H_{WA}^2}{2} B_A (1 - \xi) - \frac{\gamma H_{WC}^2}{2} B_C + \frac{\gamma H_{WA}^2}{2} (B_C - B_A (1 - \xi)) + \gamma \left(\frac{H_{WC} B_C + H_{WA} B_A (1 - \xi)}{2} \right) L_1 S_o - \rho \left(\frac{V_{WA}^2}{C^*} \right) (B_A (1 - \xi) + y_A) L_1 \quad (2-14)$$

and for the lateral channel control volume:

$$\rho Q_{WB} V_{WB} - \rho Q_{WB} V_{WA} = \frac{\gamma H_{WA}^2}{2} B_A \xi - \frac{\gamma H_{WB}^2}{2} B_B + \frac{\gamma H_{WA}^2}{2} (B_B - B_A \xi) + \gamma \left(\frac{H_{WB} B_B + H_{WA} B_A \xi}{2} \right) L_2 S_o - \rho \left(\frac{V_{WA}^2}{C^*} \right) (B_A \xi + y_A) L_2 \quad (2-15)$$

The conservation of mass equation at either a combining or a dividing junction can be written as:

$$Q_{WC} + Q_{WB} = Q_{WA} \quad (2-16)$$

These equations, together with the St. Venant equations used for the single channels connected at the junction are used to estimate the discharge and water depth at the three sections just upstream and downstream of a junction.

2.2.3 HEC-RAS

The final model used in the proposed integrated modelling methodology was *HEC-RAS* for generating ice jams in the Hay River delta. *HEC-RAS* solves the profile of an ice jam using the ice jam force balance equation:

$$\frac{d(\bar{\sigma}_x t_i)}{dx} + \frac{2\tau_b t_i}{B} = \rho_i g S t_i + \tau \quad (2-17)$$

where:

$\bar{\sigma}_x$ = the longitudinal stress;

τ_b = the shear resistance of the banks;

and other symbols are the same as previously defined.

With some manipulation, equation (2-17) can be rewritten in the similar form as the ice jam stability equation (2-5).

$$t_i \frac{\partial t_i}{\partial x} = \frac{\tau}{2K_x \gamma_e} + \left(\frac{g \rho_i S_w}{2K_x \gamma_e} \right) t_i - \frac{\tan \phi k_1}{B} t_i^2 \quad (2-18)$$

where k_1 = the coefficient of the lateral thrust. Coincidence between equations (2-18) and (2-5) can be found when $k_1 K_x = 1$. Equation (2-18) is then solved together with the energy equation in a

similar way as described previously for the *RiverID* Ice Jam Release model. The energy equation is written as follows:

$$Z_2 + Y_2 + \frac{a_2 V_2^2}{2g} = Z_1 + Y_1 + \frac{a_1 V_1^2}{2g} + h_e \quad (2-19)$$

where:

Z_1, Z_2 =elevation of the main channel inverts (m);

Y_1, Y_2 =depth of water at the cross sections (m);

V_1, V_2 =average velocities (m^2/s);

a_1, a_2 =velocity weighing coefficients (*dimensionless*);

and h_e =energy head loss (m).

2.3 Integrated Modelling Method

To incorporate the effects of upstream ice jam release waves into the prediction of flood levels within the Hay River Delta, a new integrated modelling method was developed which utilizes a series of 1-D models: the *RiverID* Ice Jam Release Model, the *RiverID* Network Model, and the *HEC-RAS* model. The *RiverID* Ice Jam Release model was used first to simulate the propagation of an ice jam release wave in the Hay River upstream of the delta. Discharge measured at the EMO Alexandra Falls gauge station was used as the upstream boundary condition and the water level at the WSC Great Slave Lake gauge was used as the downstream boundary condition. Although the reach modelled within the ice jam release model extends to the lake, the model was not expected to produce accurate results for the multi-channel reach within the delta. Thus, a hydrograph was output at the Forks (km 1108) for use as an upstream boundary

condition in the *River1D* Network model to simulate the propagation of the wave through the delta.

The Network model is currently capable of determining the wave propagation throughout the channels of the Hay River Delta but cannot calculate ice jam profiles, so *HEC-RAS* was utilized for this need. The Network model was used to determine the flow boundary conditions of each of the individual channels required by the *HEC-RAS* model in calculating ice jam profile calculations. By iterating between the two models, a pre-wave ice jam profile matching the top of ice profile of an observed jam in the delta was established. The calculated pre-wave profile was configured in the Network model as a specified ice condition. The hydrograph at the Forks calculated from the ice jam release model was then propagated through the delta with the pre-wave ice jam in place. Hydrographs of the propagated release wave were output from both the East and West channels just downstream of the Forks to be used as boundary conditions in the *HEC-RAS* model to calculate post-wave arrival ice jam profiles. As *HEC-RAS* only simulates steady flow and final ice jam profiles, the peak flows were used in place of the full wave hydrograph. It had been shown by She et al. (2008) that the peak flow alone is often adequate to produce reliable water and ice jam profiles, justifying the use of these peak flows in modelling post-wave jam configurations. The toe location was manually adjusted in *HEC-RAS* to simulate the observed jam shift. A final post-wave ice jam profile was then modelled. A flow chart of this method is shown in Figure 2.3.

2.4 Modelling Domain

Open water survey programs were conducted by the University of Alberta in the summers of 2005, 2007, and 2008, obtaining measurements for flow velocities, discharges, and

water levels at specific points in the Hay River Delta, as well as bathymetry. The first survey, conducted in August of 2005, consisted of the gathering of bed and bank data in the Hay River Delta up to 1112.2 km in the East Channel and 1111 km in the West Channel. The second survey conducted in July 2007 extended this bathymetry through the channels into the Great Slave Lake, and the final survey conducted in September of 2008 gathered more bathymetric data close to the West Channel Bridge.

Both *River1D* Ice Jam Release and the *River1D* Network model employ a “limited geometry approach,” requiring a rectangular approximation of the river. The rectangular geometry is available from previous studies (U of A River Ice Research Group) for the upper reach of the Hay River (km 1000 to 1114) and is adapted here. There are a total of 503 cross sections with 200-250 m space interval. For the delta channels, the surveyed bathymetric data of the delta was used to develop the rectangular cross sections. The *River2D* model of the delta was run with a 1:2 year flood to obtain a water surface whose width was used as the width of the approximated rectangular cross section. The modelled hydraulic mean depth (flow area/top width) was subtracted from the computed 1:2 year water surface elevation to get the effective bed elevation for the rectangular cross section. 1600 cross sections were spaced at 10 m intervals such that variations in the elevations of the channels would be captured in the model. The layout of the *River1D* Network model of the delta can be seen in Figure 2.4.

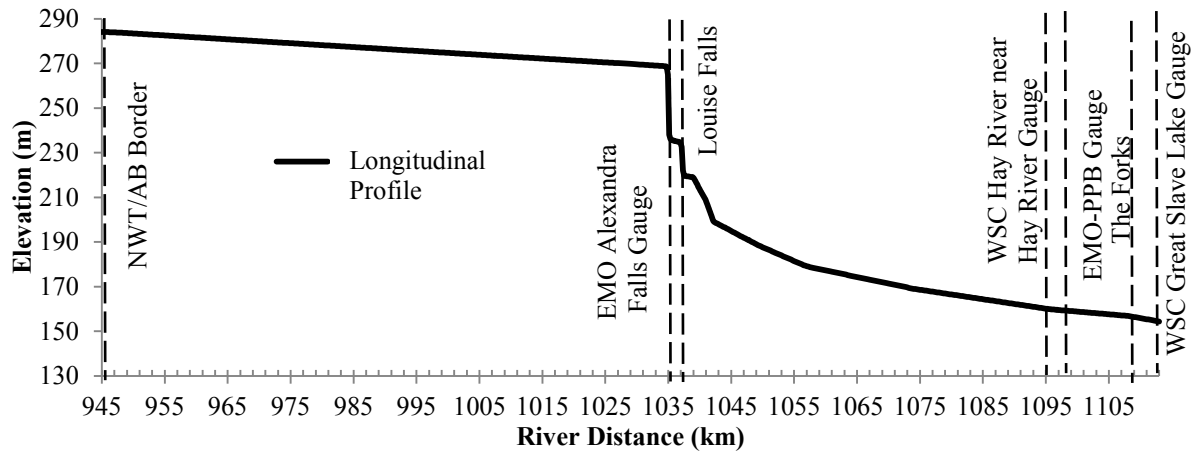


Figure 2.1 Bed profile of equivalent rectangular channel for the Hay River showing key landmarks and gauge stations (Adapted from Hicks et al., 1992).

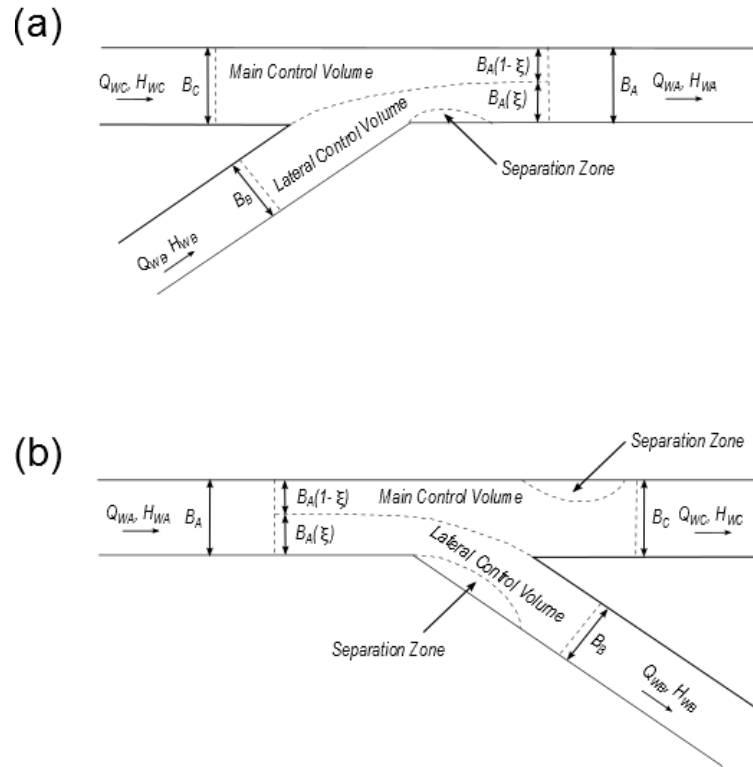


Figure 2.2 Open channel junction configurations for (a) combining junction and (b) dividing junction (adapted from Shabayek 2002).

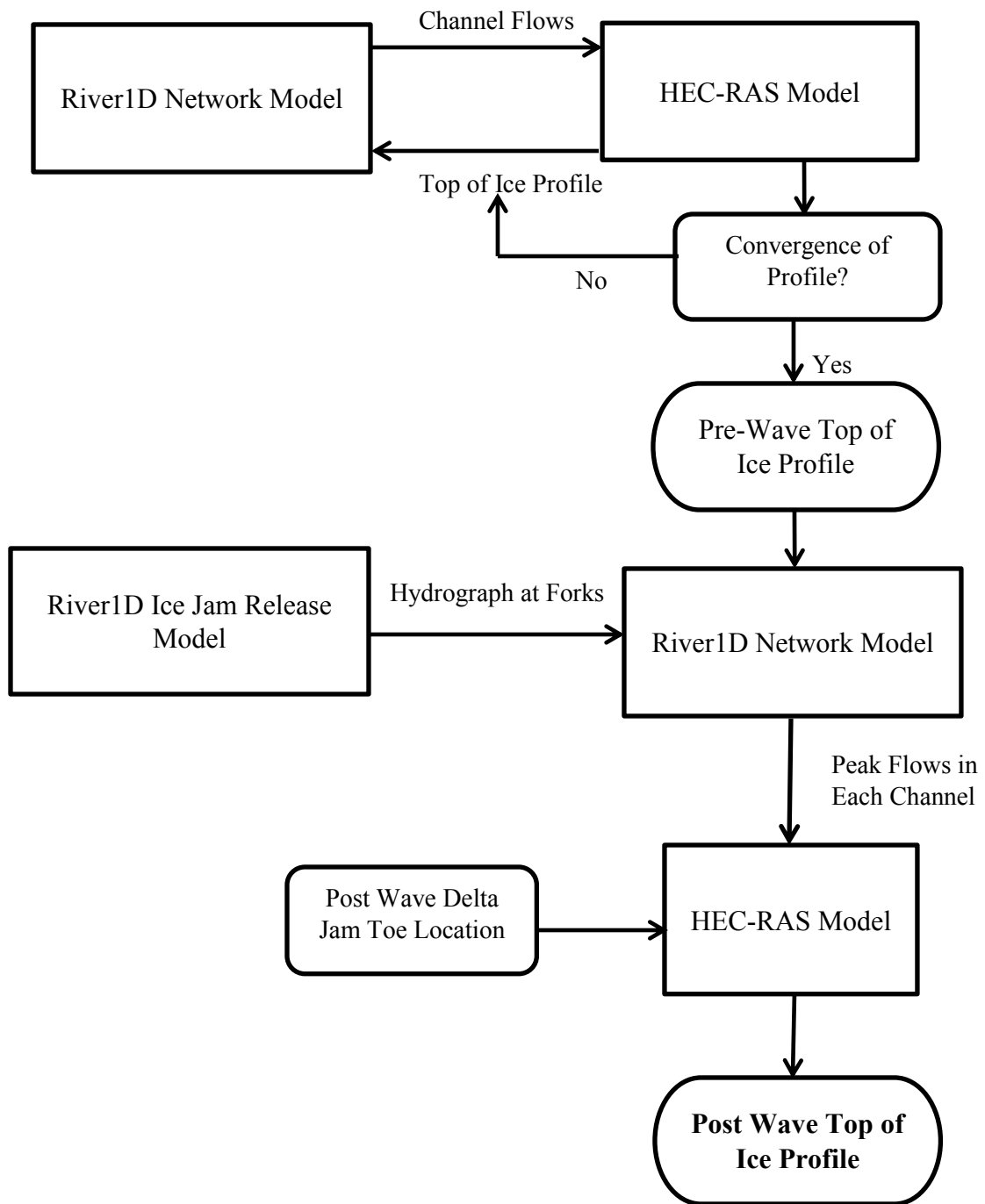


Figure 2.3 Flowchart of integrated modelling method.

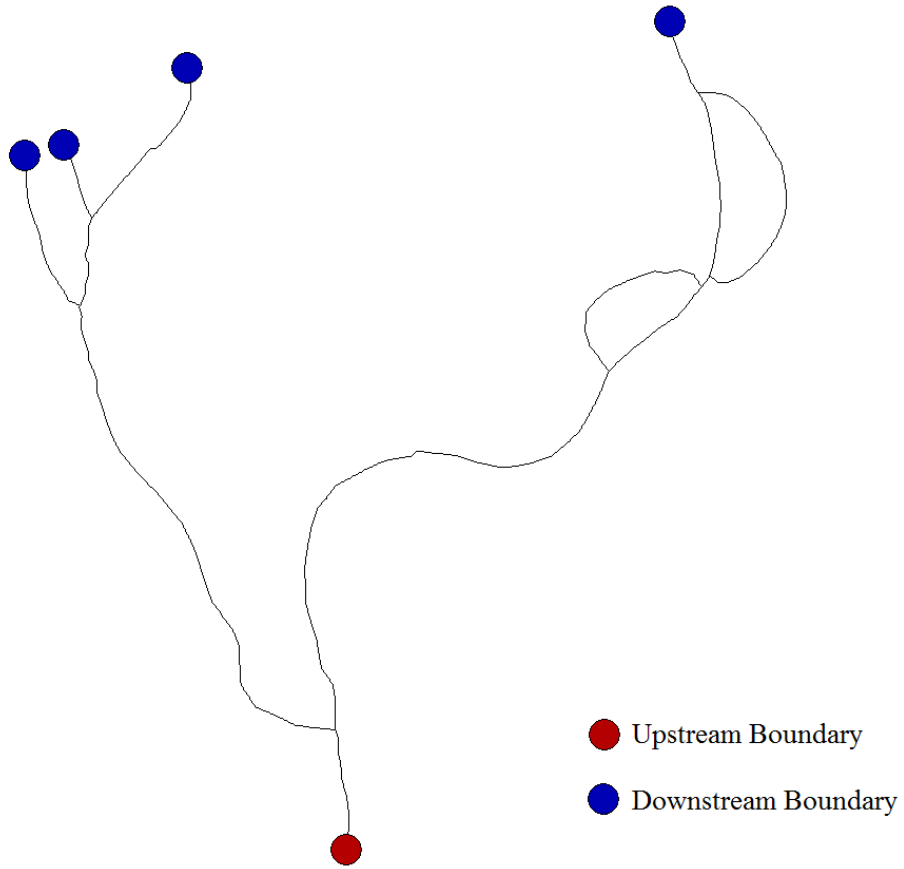


Figure 2.4 Plan view schematic of River1D Network model geometry of Hay River Delta.

Chapter 3 : Calibration and Validation

3.1 Validation of *River1D* Network Model

The *River1D* Network model has only been applied in hypothetical simulations previously (Blackburn et al., 2015), thus it was first validated under both open water and specified ice conditions. A Manning's n value of 0.025 was used for the channel bed resistance based on calibrations conducted by Brayall and Hicks (2012) for the same reach.

Discharges in the individual channels of the delta were measured with an Acoustic Doppler Current Profiler (ADCP) during the summer of 2007 under open water conditions (Brayall and Hicks, 2012). The locations of the cross sections these measurements were taken at are detailed in Figure 3.1. The closure in these measurements was deemed good when comparing section 1 to the sum of sections 2 and 3, as well as comparing section 3 to section 5 and 6. The closure between section 2 and 4 is weaker however, because of the low flow velocities experienced at section 4 stemming from its closeness to the mouth of the river at Great Slave Lake, creating measurement errors in ADCPs. The measured inflow into the Delta of $245 \text{ m}^3/\text{s}$ was set as the upstream boundary condition in the *River1D* Network model and the flow apportionment between the individual channels was calculated. The model calculated discharges are compared with the ADCP measurements at the corresponding cross sections, as shown in Table 3.1. Good agreement was found between the measurements and modelled values, with a maximum error $\leq 4.2\%$, except for cross section 4, containing an error of 7.8% due to the difficulty of attaining closure and possible error in the measured discharge.

Table 3.1 Comparison of modelled flow splits to 2007 ADCP measurements.

	Location	Modelled Flow (m ³ /s)	Measured Flow (m ³ /s)	% Difference
1	The Forks	245	245	0*
2	East Channel	194	195	0.5
3	West Channel	51	49	4.1
4	East Channel	194	180	7.8
5	Rudd Channel	25	24	4.2
6	Fishing Village Channel	26	25	4.0

* Upstream boundary condition in the *River1D* Network model

The *River1D* Network model of the delta was also validated under a set of ice conditions by comparing to the *River2D* model. A relationship between the total inflow discharge to the delta and the East Channel discharge under ice conditions was previously developed by calibrating a *River2D* model for 11 historic ice jam events (Brayall and Hicks, 2012). A similar relationship was developed using the *River1D* Network model by setting the historical ice jams as specified ice conditions. As discharge measurements were not available in the channels of the delta for ice affected events, this model to model comparison was necessary to validate the accuracy of the flow split in these conditions. Figure 3.2 provides a comparison between the relationships developed using the two models. The results of the *River1D* Network model compared favorably to those of the *River2D* model, with an average difference of 3.4% and a maximum difference of 5.5%.

3.2 Breakup Modelling

Detailed monitoring of breakup events in the Hay River Delta was carried out by the University of Alberta in 2008 and 2009, focusing on the acquisition of inflow discharge, ice surface elevations, and ice jam length and locations for modelling ice jams that occurred in the

reach. The discharge measurements were sourced from two gauge stations, EMO Alexandra Falls and WSC Hay River near Hay River. Lake level was obtained from WSC Great Slave Lake at Hay River. The top of ice elevation profile of the delta jams was measured using a Real Time Kinematic GPS when the ice jams were stable and accessible. Additional observations were conducted using aerial photography to better document the location of ice jams in the Delta as well as the progression of ice runs from the upstream portions of the Hay River. An example of these aerial photos can be seen in Figure 3.3 below.

The proposed modelling method was validated using the 2008 and 2009 breakup events. In both years ice jams in the upstream reaches of the Hay River released, sending a wave of water and ice downstream. The arrival of this wave caused the ice jam in the delta to shift downstream, consolidating and lengthening the ice jam in both cases. The toe location and length of the upstream jam, as well as its release time, were observed. The ice surface elevation profile for the delta jams was measured both before and after the arrival of the release wave.

3.2.1 2008 Breakup

The 2008 breakup occurred at the end of April and the beginning of May, with the first ice movement in the Hay River Delta observed late on May 4. By the morning of May 5, small ice accumulations were observed toed at km 1111 in the East Channel and against the intact lake ice in the West Channel (Brayall and Hicks, 2012). On May 5, 2008 at 10:30, an approximately 9 km long ice jam was observed toed at river station km 1103 just upstream of the Forks. The ice conditions upstream and within the delta are shown in Figure 3.4. Based on the WSC Hay River near Hay River and EMO Pine Point Bridge gauges, the release of this ice jam was estimated to occur at 19:15 on May 5. At approximately 20:10, the ice jam in the East Channel was pushed

downstream by 0.55 km and the jam significantly lengthened and thickened. This ice jam remained in place over May 6 and resulted in severe flooding. During the time span of this breakup event, several top of ice surveys were conducted in the delta. The profiles surveyed on May 5 and May 6 were deemed representative of the conditions before and after the arrival of the ice jam release wave.

The 9 km ice jam upstream of the delta was observed from reconnaissance flights of the river (Watson et al. 2009) but its profile was not measured. Therefore, the initial ice jam profile was calibrated against water levels measured at two gauges at km 1095 (WSC Gauge of Hay River at Hay River) and km 1098 (EMO Pine Point Bridge Gauge), both located within the length of the ice jam. Figure 3.5 shows the magnitude of water level increase caused by the ice jam as calculated from *RiverID* and measured from the two gauge stations. The calibrated ice jam underside roughness Manning's n was 0.05. For the release of this ice jam, the empirical parameters describing the ice resistance and dispersion effects λ_1 and λ_2 were calibrated to be 3 and 0, respectively, which best modelled the wave travel time from the release location to the delta estimated based on field observations. The bank resistance parameter (λ_I) was previously found to range from 0 to 3.5 for accurate modelling of the propagation of release waves on various rivers (She and Hicks, 2006). The calibrated value of 3 was considered reasonable as the distance from the release location to the delta was within two jam lengths, indicating the effects of bank resistance were significant. The hydrograph at the Forks was output from the *RiverID* Ice Jam Release model and used as the upstream boundary condition in the *RiverID* Network model, in which it was then routed downstream in the delta channels. The modelled hydrograph at the Forks, as well as the hydrographs in the East and West Channel just downstream of the

Forks, are depicted in Figure 3.6. Approximately 65% of the flow went into the East Channel and 35% into the West Channel.

Ice jam profiles in the delta channels were calculated using *HEC-RAS*. Carrier discharge before the ice jam release was used for calculating the pre-wave profile while the peak discharges from the *River1D* Network model were used for simulating the post-wave profile. In calibrating with the pre-wave survey, a Manning's n of 0.06 was used for the underside roughness of the delta ice jam. The same value was used in modelling the post wave jam. The toe location was manually moved from km 1111 as for pre-wave jam to km 1111.55 for post wave jam. Figures 3.7 and 3.8 show the modelled ice jam profiles in the East Channel and the West Channel respectively, both before and after the wave arrival. The top of ice profile was surveyed for the East Channel jam both before and after wave arrival, and for the West Channel post wave jam only. These measurements are also shown in the figures for comparison. The computed elevation of the top of the ice compares favorably to that of the field measurements in both channels of the delta, with an average difference of 0.27 m in the East Channel and 0.32 m in the West Channel.

3.2.2 2009 Breakup

Much like the 2008 event, the 2009 breakup also began in early May, with ice movement first observed at approximately 02:00 on May 3. Small ice accumulations within the delta were observed on the same day. After some minor consolidation events, the delta ice jams toed at around km 1112 in both East and West Channels on May 5. A sequence of three ice jams in the upper reach of the Hay River was first observed at 14:00 on May 4, one 1.4 km long toed at km 1049, one 1.1 km long toed at km 1047.1, and one 4.3 km long toed at km 1045. They later

released at 2:00 on May 6, sending a release wave downstream to the small ice jams in the delta. The ice conditions both upstream and within the delta are shown in Figure 3.9. Ice movement in the delta was observed at around 5:00 on May 6. By May 7, the ice jam had shifted even further downstream the East Channel, nearly reaching the mouth of Great Slave Lake. During this event, surveyors measured eight top of ice jam profiles throughout the progression of breakup in both the East Channel and the Fishing Village and Rudd Channels of the West Channel. The surveyed top of ice profile on May 5 and May 7 were deemed representative of the pre-wave and post-wave ice jam conditions in the delta. Like the 2008 breakup, both pre-wave and post wave profiles were surveyed for the East Channel ice jam but only a post wave profile was surveyed for the West Channel ice jam.

The release of the three ice jams upstream had been modelled in a previous study with the *RiverID* Ice Jam Release model (Watson et al., 2009) and the same parameters were used here. Underside roughness of the released jams was set to 0.06, and both λ_1 and λ_2 were set to 0. The toe of the furthest downstream ice jam was over 50 km upstream of the Hay River Delta, so effects of ice resistance would no longer affect the wave by the time it reached the delta. Again, the hydrograph at the Forks was output from the *RiverID* Ice Jam Release model. It is shown in Figure 3.10 along with the hydrographs in the East and West channels as calculated by the *RiverID* Network model. Approximately 65% of the flow went into the East Channel and 35% into the West Channel.

Ice jam profiles in the delta channels were calculated using *HEC-RAS*. Carrier discharge before the ice jam release was used for calculating the pre-wave profile while the peak discharges from the *RiverID* Network model were used for simulating the post-wave profile. Calibrated against the pre-wave ice jam surface profile, a Manning's n of 0.05 was used for the

underside roughness of the delta ice jam. The same values were used for the post-wave jam with the jam toe shifted from km 1112.36 to km 1113.22. The modelled ice jam profiles together with the surveyed top of ice profiles in the East Channel and West Channel are shown in Figure 3.11 and Figure 3.12. The post-wave profiles in the Delta compared favorably with those measured for this event, with an average distance of 0.19 m in the East Channel and 0.14 m in the West Channel, apart from some higher observation values linked to the inability of the 1-D model to capture the 2-D transverse variations in the top of ice elevations.

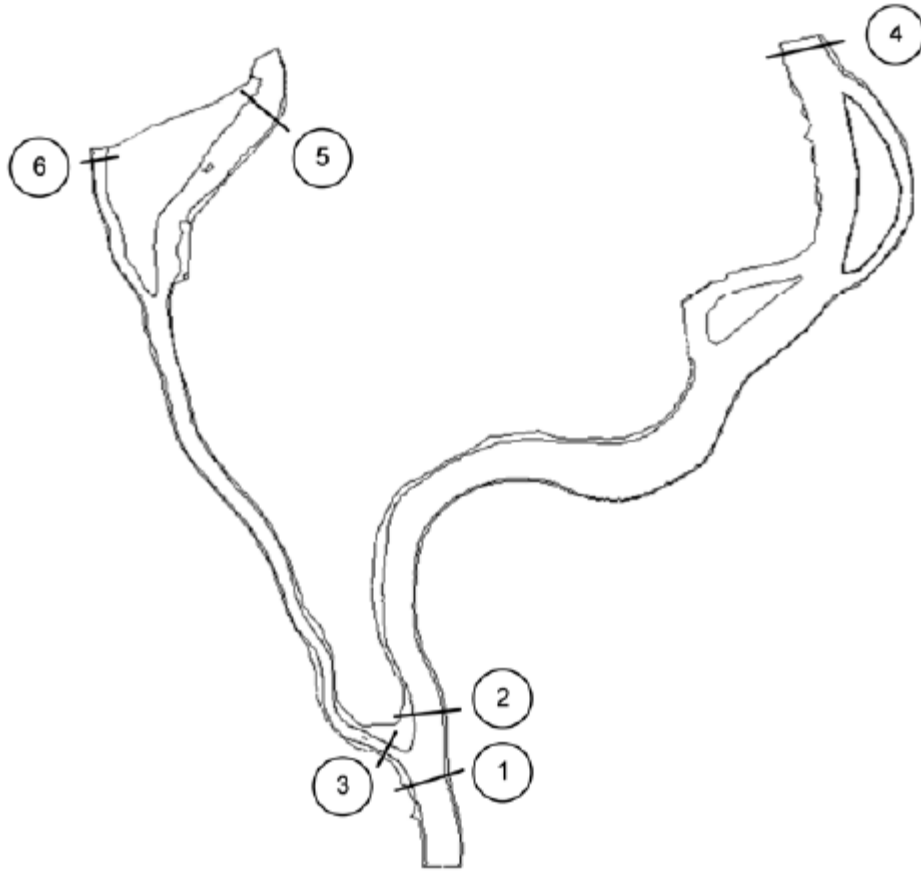


Figure 3.1 Locations of ADCP cross sections in the Hay River Delta (Brayall 2011).

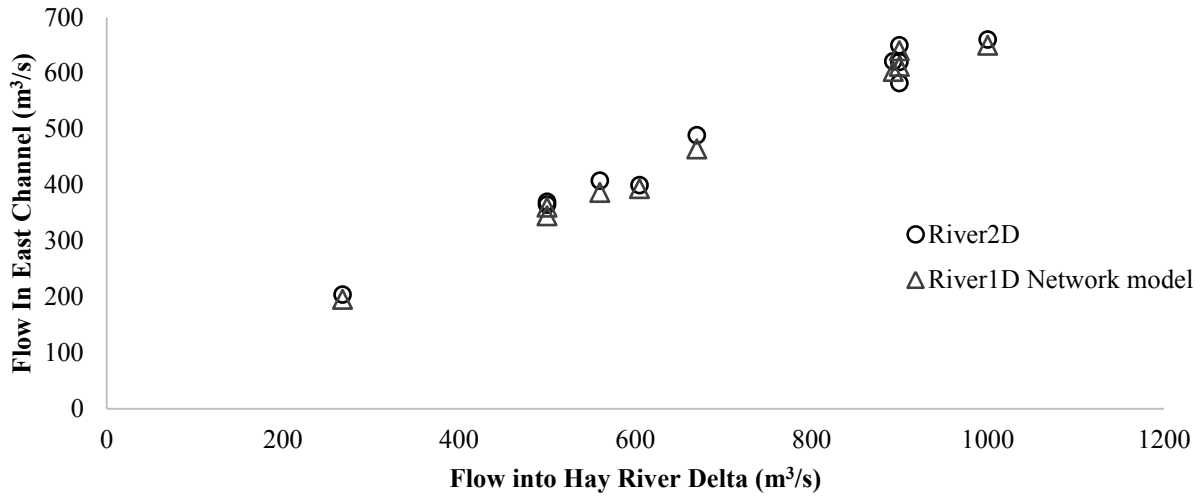


Figure 3.2 Comparison of flow apportionment into East Channel between *River1D* Network model and *River2D* (Brayall and Hicks, 2012).



Figure 3.3 Example aerial photo of ice jam in the East Channel of the Hay River Delta taken May 5, 2008 (Brayall 2011).

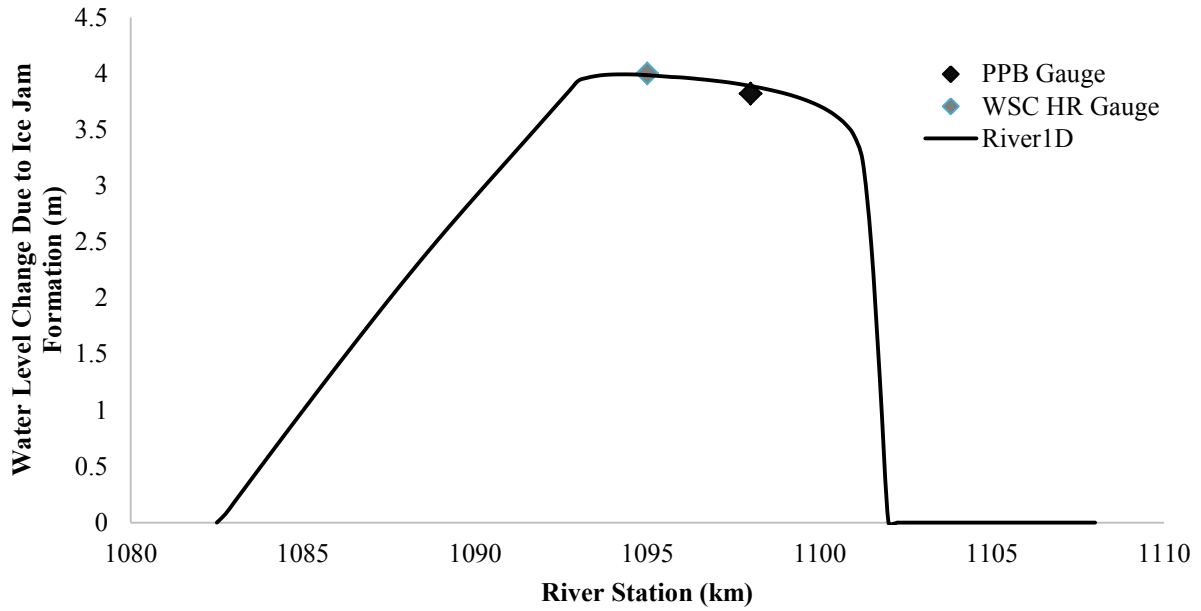


Figure 3.4 Calibration of 2008 upstream ice jam using data from WSC Hay River near Hay River and EMO gauge at Pine Point Bridge.

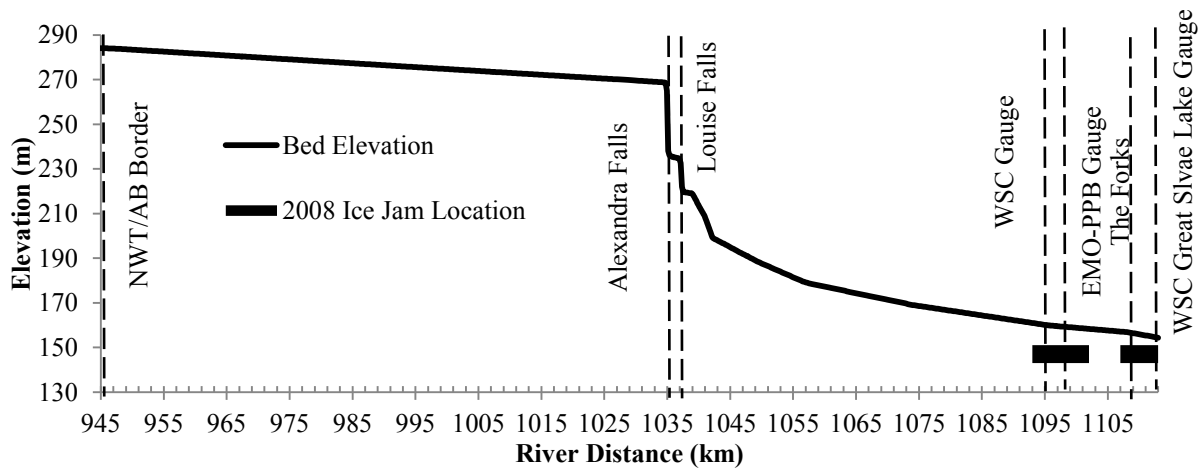


Figure 3.5 Ice Jam Map for modelled 2008 release (adapted from Hicks et al., 1992).

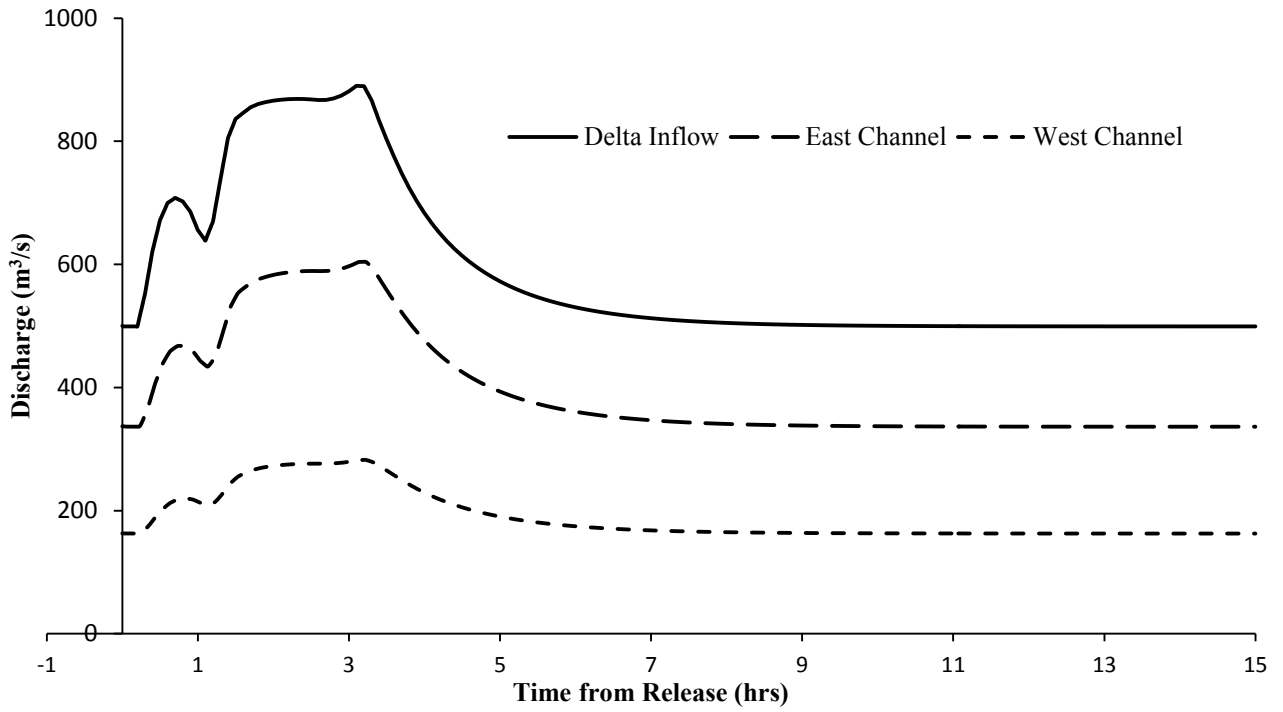


Figure 3.6 Ice jam release hydrograph for the 2008 release event modelled with the *River1D* Network model.

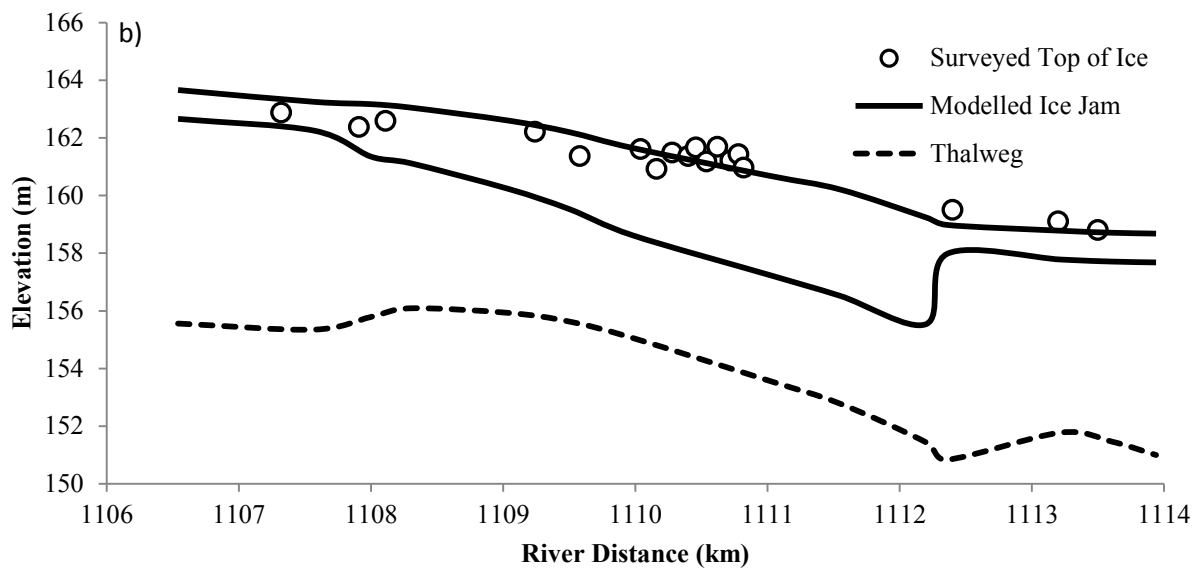
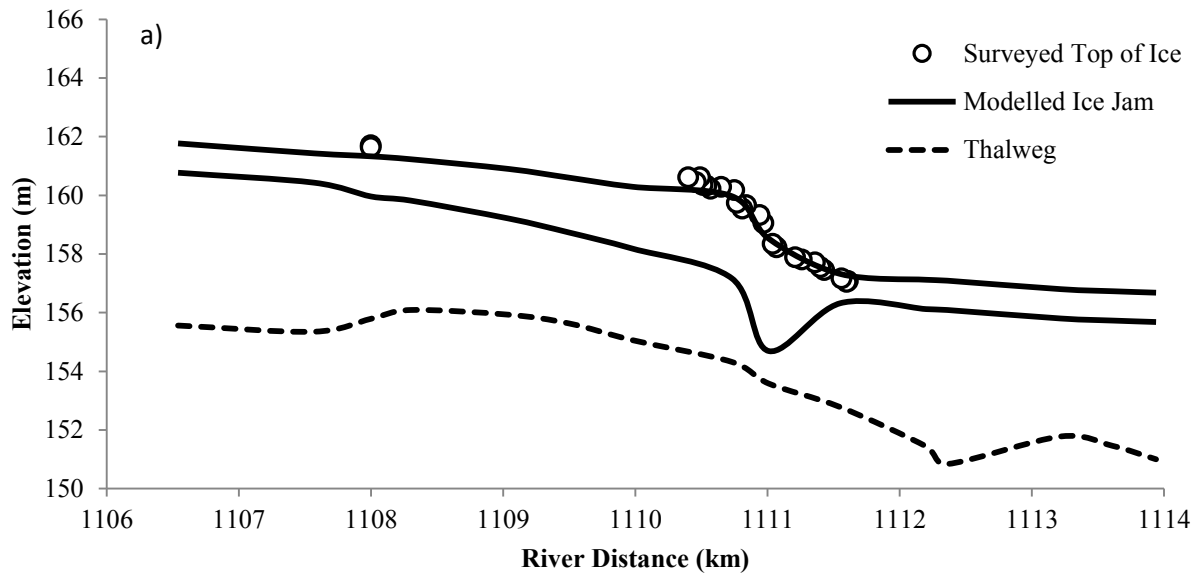


Figure 3.7 Pre a) and post b) wave delta ice jam configurations for East Channel-2008.

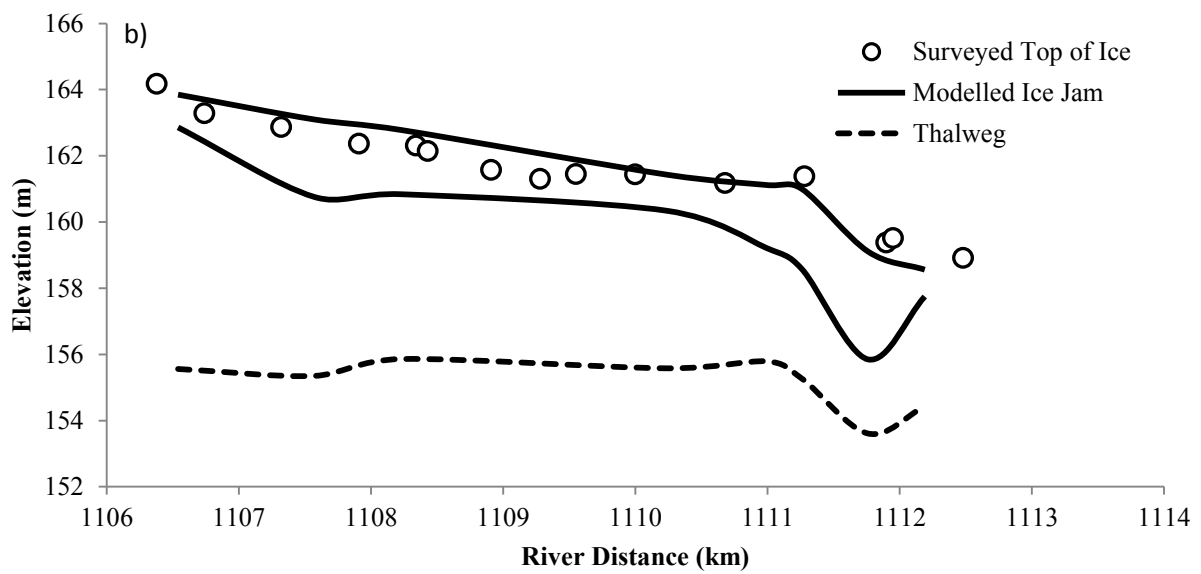
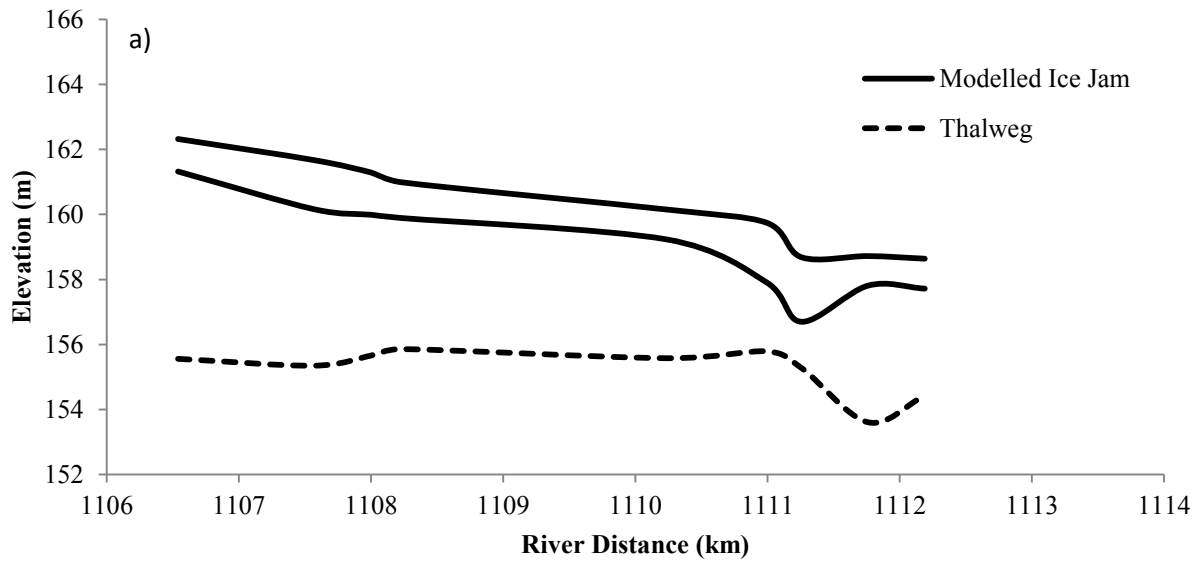


Figure 3.8 Pre a) and post b) wave delta ice jam configurations for West Channel-2008.

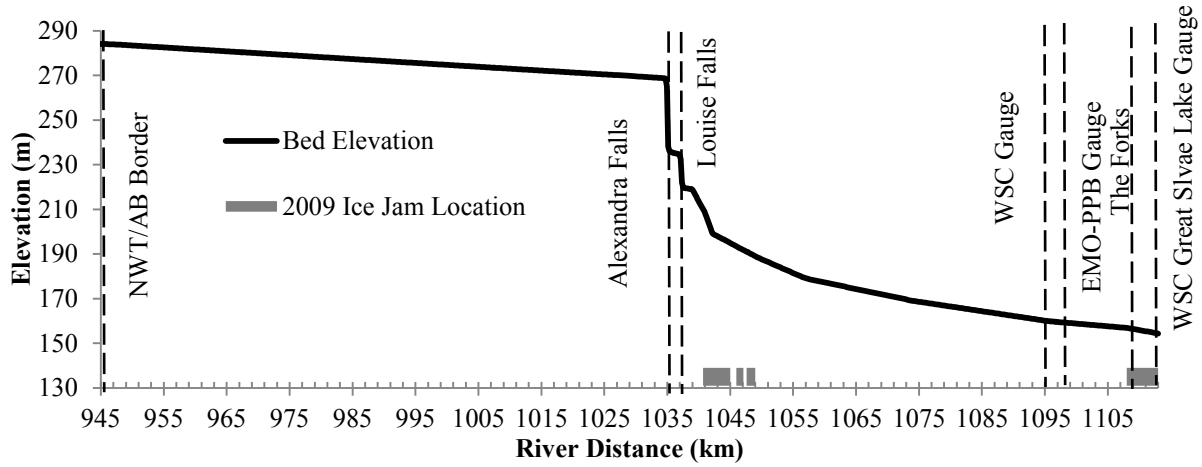


Figure 3.9 Ice Jam Map for modelled 2009 release (adapted from Hicks et al., 1992).

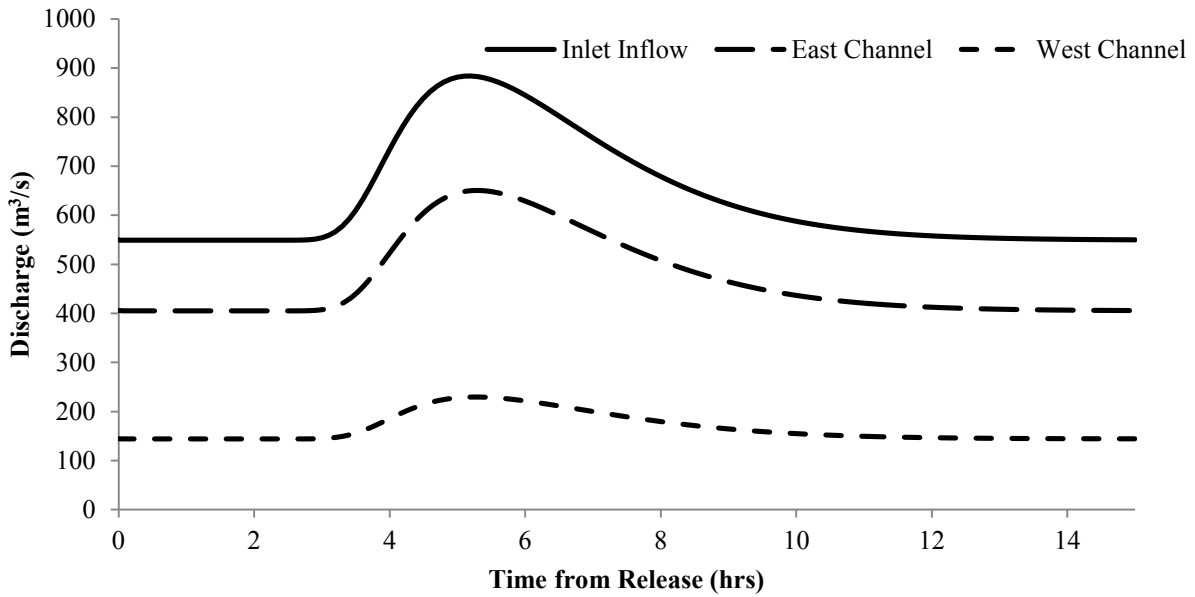


Figure 3.10 Ice jam release hydrograph for the 2009 release event modelled with the *RiverID* Network model.

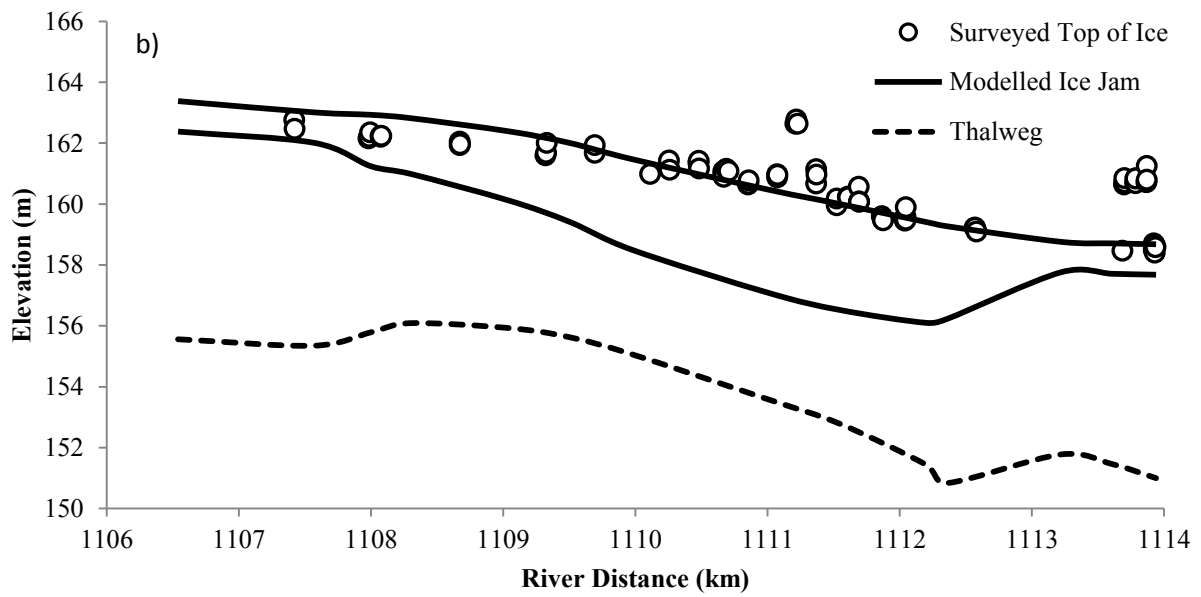
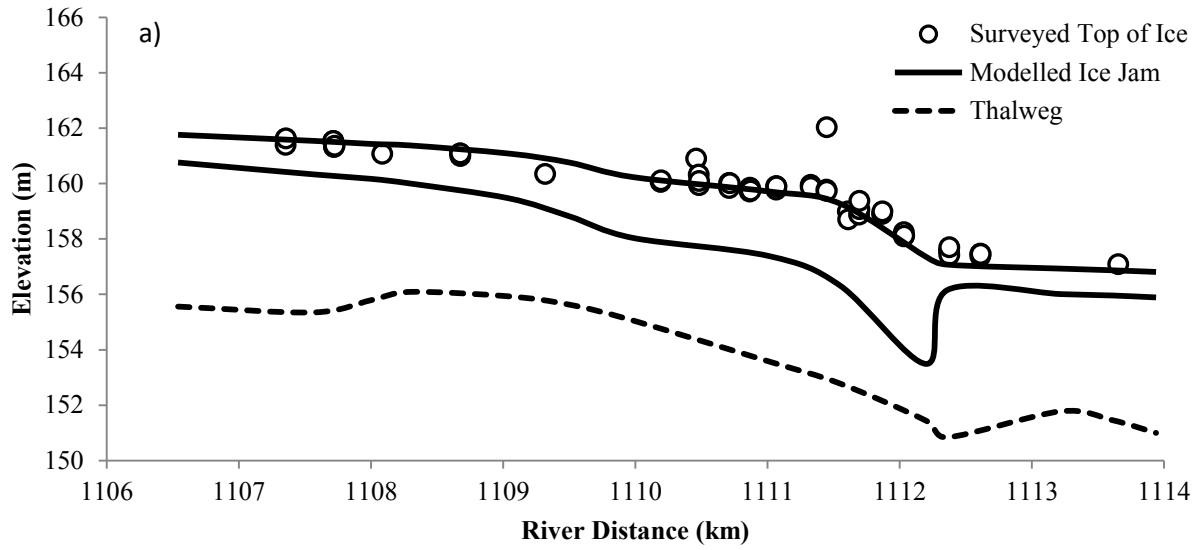


Figure 3.11 Pre (a) and post b) wave delta ice jam configurations for East Channel-2009.

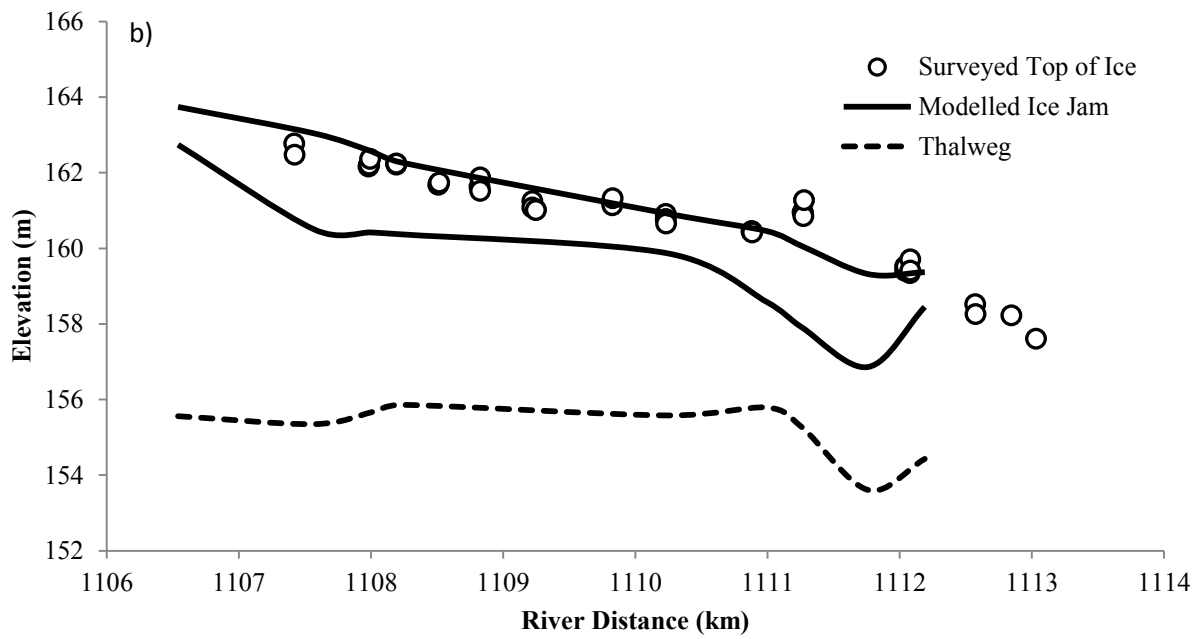
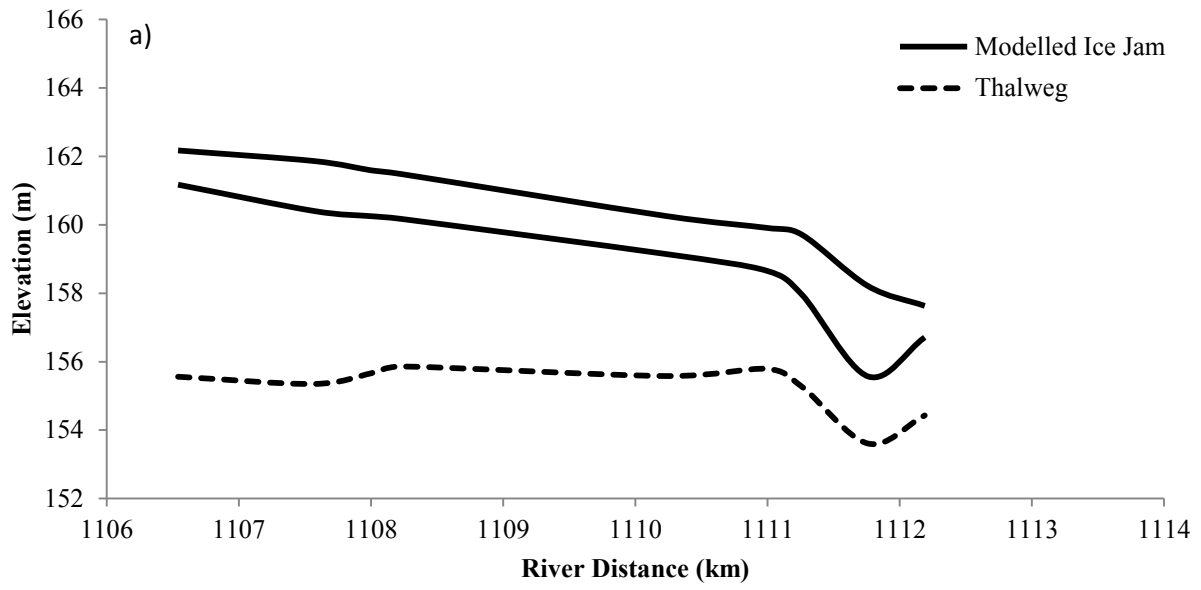


Figure 3.12 Pre (a) and post b) wave delta ice jam configurations for West Channel-2009.

Chapter 4 : Model Application

4.1 Hypothetical Scenarios

The validated new modelling methodology was then used to simulate a series of hypothetical events. The top of ice profiles obtained from these events would provide a data set that was then statistically analysed to develop relationships between the variables defining them and the resulting profiles. These relationships would form the basis of a flood level prediction tool in the delta. The East Channel was focussed on due to the large amount of data available for this channel; however, the same method could easily be applied to the West Channel. Each hypothetical event modelled consisted of a unique combination of upstream ice jam configuration and delta jam configuration. Five key variables were identified: the length and toe location of the upstream ice jam, the carrier discharge at release, the distance of the toe shift of the delta ice jam in the East Channel, and the water level at the Great Slave Lake. These variables have direct effect on either the peak flow in the delta caused by upstream ice jam release or the potential severity of the post wave jam. Additionally, with the exception of the delta jam toe shift, each of these variables can be measured in the field well in advance of any flooding events that may occur in the delta, making them ideal for use in a flood prediction tool. Multiple configurations of the pre-wave delta ice jam were also tested, with the jam length ranging from 3-5 km, the toe location ranging from km 1110-1112, and the lake level ranging from 156.6 m to 158.6 m. These tests showed that for the same incoming wave hydrograph, the percentage of discharge entering the East Channel of the delta was only affected by the different pre-wave jam condition for approximately 0.5 to 3.0%. This indicated that the pre-wave jam configuration has minimal effect on the flow apportionment between the East and West Channels. As the peak discharge in each individual channel decides the post wave jam

configuration, a single pre-wave jam across all hypothetical events was deemed adequate. The underside roughness of both the upstream ice jam and the delta jam used a Manning's n of 0.06. λ_1 and λ_2 were set based on the 2008 and 2009 model validation runs, i.e. $\lambda_1 = 3$ and $\lambda_2 = 0$ if the distance between the release location and the delta was within 2 jam lengths and $\lambda_1 = 0$ and $\lambda_2 = 0$ otherwise.

Historical records were reviewed for selecting a range of values of each key variable. The largest discharge recorded on the Hay River during breakup was 1240 m³/s, occurred on May 2, 1974, in the WSC gauge records. The range of simulated carrier discharges was 200 m³/s to 1200 m³/s with 200 m³/s increments. Documented historical ice jams in the upper reaches of the Hay River were reviewed, with the relevant information listed in Table 4.1 (Gerard and Stanley, 1988, Kovachis 2011). It was noticed that ice jams in these records with a length exceeding 10 km all melted in place. Therefore, the longest simulated upstream ice jam was 10 km. Four jam lengths, 2.5 km, 5 km, 7.5 km, and 10 km were simulated in the hypothetical events. Typical toe locations of the upstream ice jam were also reviewed. The most downstream location considered was km 1100, as jams have been rarely observed between this location and the entrance of the delta. To determine the upper limit of the toe location, a few simulation runs were conducted and it was shown that ice jams toed upstream of Alexandra Falls all produced lower or similar peak flows at the delta. Because of this, the most upstream toe location considered was km 1020. The modelled toe locations were placed at 10 km intervals except for the region containing Alexandra Falls and Louise Falls, as realistic ice jam profiles could not be generated in the model due to the steep slope and high flow velocities.

Table 4.1 List of documented historical ice jam events in the upstream reaches of the Hay River.

Year	Date	Toe Location (km)	Length (km)	Carrier Discharge (m ³ /s)	Notes
1963	April 30	1073			
1988	April 24	1055.42	14	135	Deteriorated
1988	April 26	1059.92	16	221	Deteriorated
1992	April 26	1090		309	
1992	April 28	1105		900	
2005	April 22	1048		259	
2005	April 23	1071		451	
2005	April 23	1088.5		451	
2007	April 25	1025.9	4.8	290	
2007	April 26	958.2	6.7	450	
2007	April 26	949.5	9.5	450	
2007	April 26	1103	28	450	Deteriorated
2008	May 4	992.5	6.2	450	
2008	May 4	1051	6	650	
2008	May 5	1103	9	500	Released
2009	May 5	948.6	2.6	550	
2009	May 6	1049	1.4	550	Released
2009	May 6	1047.1	1.1	550	Released
2009	May 6	1045	4.3	550	Released
2010	April 23	986		140	
2010	April 23	1040.5		140	
2011	May-05	1048	5	238	
2011	May-06	1068	5	365	
2011	May-08	1101	22	478	Deteriorated

Delta ice jam configuration was also selected based on historical observations, summarized in Table 4.2 (Gerard and Stanley, 1988, Kovachis 2011). The pre-wave jam in the delta was configured as 4.5 km long with a toe location of km 1111 in the East Channel, based on the most typical toe location in years where flooding did not occur, as well as the known toe location of the delta ice jams in 2008 and 2009 before consolidation occurred (Gerard and Stanley, 1988). Significant flooding has been associated with the shifting of ice jam toes past km 1111 in the East Channel (Gerard and Stanley, 1988). Therefore, a range of potential toe shifts

was selected moving downstream from km 1111 encompassing small to big shift distance. These toe shifts were simulated by changing the toe location of the post-wave ice jam, while keeping the same head location upstream of the delta. The modelled values of lake level ranged between 156.6 m and 158.6 m based on lake levels observed that corresponded to documented historical jam events (Brayall and Hicks, 2012). The values simulated for the five key variables are listed in Table 4.3. Each possible combination of the five key variables was simulated using the 1-D integrated modelling method described in Chapter 3. The top of ice levels were output for each scenario at an approximately 0.5 km intervals between km 1108 and km 1114.24 in the East Channel. In total 1612 unique profiles were obtained from the variables.

Table 4.2 List of documented historical ice jams in the Hay River Delta.

Year	Date	Toe (km)	Head (km)	Discharge (m ³ /s)	Flooding
1950	May 07	1111			Some
1954	May 16	1111.5		1150	None
1956	May 06	1111	1108.9		Some
1957	May 03	1112.4			Some
1963	May 01	~1112			Significant
1965	May 02	1111.15		750	Some
1974	May 01	1112.25		1100	Significant
1977	May 02	1110		500	None
1978	May 04	1111.5		793	Significant
1979	May 14	1111.5		580	Some
1985	May 05	1112.25	1107.6	1000	Significant
1986	May 04	1111.7	US Delta*	487	Significant
1987	April 29	1111	1106	965	None
1988	April 27	1110.9	1098.4	605	None
1988	April 30	1111	1104.6	353	None
1989	May 03	1112	1082	1140	Significant
1989	May 06	1111.5	US Delta	900	Significant
1990	April 28	1111	US Delta	560	None
1991		1111	US Delta	460	None
1992	April 26	1111.5		309	Significant
1992	April 28	1112.6	1105	900	Significant
2005	April 25	1111.3	1108	491	Some
2008	May 05	1110.8	US Delta	500	Significant
2008	May 06	1111.5	US Delta	893	Significant
2009	May 03	1110.8	US Delta	268	Some
2009	May 04	1111.2	US Delta	500	Some
2009	May 05	1111.8	US Delta	670	Some
2009	May 07	1111.8	US Delta	900	Some

*“US Delta” indicates an ice jam extending upstream of the delta by an unknown distance

Table 4.3 Selected values of key variables in the simulated hypothetical events.

	Release Jam Length (km)	Release Jam Toe Location (km)	Carrier Discharge (m ³ /s)	Toe Shift (km)	Downstream Lake Level (m)
1	2.5	1020	200	0.55	156.6
2	5	1030	400	1.2	157.1
3	7.5	1050	600	1.4	157.6
4	10	1060	800	2.22	158.6
5	-	1070	1000	-	-
6	-	1080	1200	-	-
7	-	1090	-	-	-
8	-	1100	-	-	-

4.2 Multiple Linear Regression (MLR) Analyses

Multiple linear regression analyses were employed to develop relationships between the simulated top of ice levels (*TOI*) in the delta region and the five selected variables, the length (*L_j*) and toe location (*T_j*) of the upstream ice jam, carrier discharge (*Q_c*), toe shift of the delta jam (*TS*), and the lake level (*LL*). The MLR analyses were applied to develop a series of regression equations at ten locations in the East Channel of the delta. These locations are the same as where the top of ice levels were output for the simulated hypothetical events. The general format of the regression equations is shown below.

$$TOI = a_1L_j + a_2T_j + a_3Q_c + a_4TS + a_5LL + a_6 \quad (4-1)$$

where a_j ($j = 1, 6$) are the regression coefficients.

Multiple equations divided around values of a single variable were found to produce better results at each location when compared to a single equation. The top of ice levels in the delta region upstream of km 1111.55 were found to be most sensitive to the carrier discharge of

the river. Therefore three regression equations were developed for each of the 5 locations in this region: one for low carrier discharges ($Q_C \leq 500 \text{ m}^3/\text{s}$), one for medium carrier discharges ($Q_C = 501 - 900 \text{ m}^3/\text{s}$), and one for high carrier discharges ($Q_C > 900 \text{ m}^3/\text{s}$). In the toe region of the jam, between km 1111.55 and 1113.22, the top of ice levels had a distinct relationship with each toe shift, thus each had an individual regression equation. At km 1113.22, the top of ice levels were sensitive to a combination of carrier discharge, downstream lake level, and toe shift. Four regression equations were developed here, two for the first three toe shifts corresponding to $LL < 157.6 \text{ m}$ and $LL \geq 157.6 \text{ m}$, and two for the largest toe shift ($TS = 2.22 \text{ km}$) corresponding to $Q_C \leq 600 \text{ m}^3/\text{s}$ and $Q_C > 600 \text{ m}^3/\text{s}$ respectively. At km 1113.6 the top of ice levels were most sensitive to the lake level, requiring only two equations, one for $LL < 157.6 \text{ m}$ and one for $LL \geq 157.6 \text{ m}$. The coefficients of the equations are summarized in Table 4.4.

Each regression equation is also associated with an average error value between the modelled top of ice elevation from the hypothetical events and the elevation predicted by the equation, a coefficient of determination indicating the closeness of fit of the equation, and a set of p-values for each variable indicating the strength of the relationship between the individual variables and the response. All the regression equations had low average errors (0.0396 m -0.431 m), relatively high values of the coefficient of determination (80-95%), and extremely low p-values (0.0001-0.0003) indicating a strong relationship between the top of ice level and the selected variables. The values of the average error for each regression equation are also listed in Table 4.4. The results of the equations at each location are shown in Figures 4.1-4.10a, presented in terms of the simulated top of ice levels versus the top of ice levels predicted by the regression equations. It can be seen that although the regression equations produced reasonable predictions of top of ice levels, there are certain levels of scatter in the figures.

Table 4.4 List of MLR equations for each location in the East Channel of the Hay River Delta.

Location (km)	Equation Criteria	a_1	a_2	a_3	a_4	a_5	a_6	Regression Error (m)
1108.3	$Q_C \leq 500 \text{ m}^3/\text{s}$	0.114	0.00885	0.00685	0.0415	0.128	129.56	0.291
	$Q_C = 501 - 900 \text{ m}^3/\text{s}$	0.173	0.0138	0.00422	0.0284	0.14	123.33	0.359
	$Q_C > 900 \text{ m}^3/\text{s}$	0.205	0.0228	0.00357	0.0685	0.164	110.29	0.322
1109.04	$Q_C \leq 500 \text{ m}^3/\text{s}$	0.104	0.00784	0.0062	0.0462	0.121	131.45	0.265
	$Q_C = 501 - 900 \text{ m}^3/\text{s}$	0.161	0.0129	0.00388	0.0397	0.139	123.98	0.342
	$Q_C > 900 \text{ m}^3/\text{s}$	0.188	0.0172	0.00342	0.0768	0.146	118.65	0.363
1109.5	$Q_C \leq 500 \text{ m}^3/\text{s}$	0.0998	0.00723	0.00588	0.0472	0.128	130.82	0.255
	$Q_C = 501 - 900 \text{ m}^3/\text{s}$	0.154	0.0122	0.00368	0.0421	0.145	123.57	0.331
	$Q_C > 900 \text{ m}^3/\text{s}$	0.183	0.0165	0.0033	0.0752	0.151	118.27	0.352
1109.98	$Q_C \leq 500 \text{ m}^3/\text{s}$	0.0988	0.00681	0.00571	0.0161	0.163	125.37	0.252
	$Q_C = 501 - 900 \text{ m}^3/\text{s}$	0.147	0.0113	0.00344	0.0009	0.163	121.44	0.318
	$Q_C > 900 \text{ m}^3/\text{s}$	0.175	0.0155	0.00314	0.0138	0.158	117.85	0.337
1111.01	$Q_C \leq 500 \text{ m}^3/\text{s}$	0.0972	0.00626	0.00542	-0.0543	0.143	128.34	0.252
	$Q_C = 501 - 900 \text{ m}^3/\text{s}$	0.14	0.0104	0.00318	-0.106	0.165	121.6	0.313
	$Q_C > 900 \text{ m}^3/\text{s}$	0.168	0.0144	0.00295	-0.0727	0.176	115.5	0.322

Table 4.4 List of MLR equations for each location in the East Channel of the Hay River Delta (continued).

Location (km)	Equation Criteria	a_1	a_2	a_3	a_4	a_5	a_6	Regression Error (m)
1111.55	$TS = 0.55$ km	0.114	0.00597	0.00309	n/a	0.163	124.86	0.462
	$TS = 1.2$ km	0.137	0.0104	0.00396	n/a	0.0726	134.75	0.356
	$TS = 1.4$ km	0.132	0.0104	0.00381	n/a	0.0862	132.71	0.334
	$TS = 2.2$ km	0.138	0.0111	0.00393	n/a	0.135	124.1	0.352
1112.2	$TS = 0.55$ km	0.0422	0.00043	0.00111	n/a	0.671	50.9	0.223
	$TS = 1.2$ km	0.102	0.00651	0.00241	n/a	0.51	69.33	0.354
	$TS = 1.4$ km	0.132	0.0103	0.00368	n/a	0.0668	135.21	0.339
	$TS = 2.2$ km	0.142	0.0118	0.00416	n/a	0.1	128.12	0.372
1112.36	$TS = 0.55$ km	0.04	0.00046	0.00106	n/a	0.684	48.76	0.209
	$TS = 1.2$ km	0.0545	0.00473	0.00163	n/a	0.817	23.34	0.262
	$TS = 1.4$ km	0.115	0.00704	0.00301	n/a	0.541	63.94	0.382
	$TS = 2.2$ km	0.142	0.0119	0.00417	n/a	0.0973	128.39	0.376
1113.22	$LL < 157.6$ m & $TS < 2.2$ km	0.0228	0.00114	0.0009	0.00052	0.695	46.38	0.0921
	$LL \geq 157.6$ m & $TS < 2.2$ km	0.0358	0.00371	0.00088	0.158	0.689	44.42	0.167
	$Qc \leq 600$ m ³ /s & $TS = 2.22$ km	0.0599	0.00377	0.002	n/a	0.976	-1.14	0.264
	$Qc > 600$ m ³ /s & $TS = 2.22$ km	0.115	0.0114	0.00239	n/a	0.538	59.24	0.313
1113.6	$LL < 157.6$ m	0.0125	0.00067	0.00048	0.00014	0.832	25.45	0.0522
	$LL \geq 157.6$ m	0.021	0.00182	0.00044	0.034	0.831	24.36	0.0868

Reviewing the simulation results for the hypothetical scenarios revealed that linear relationship is not always a good approximation of the relationship between the top of ice levels within the delta and the selected key variables. This was especially true for the toe location of the upstream jam (T_i). It was noticed that in general, the closer the toe of the upstream jam to the delta, the higher the top of ice levels are in the delta. However, there are some exceptions. Ice jams toed at km 1020 consistently produced greater peak flows at the Forks, thus higher top of ice levels in the delta, than those toed at km 1050, and in some cases those toed at km 1060, due to the river geometry and resulting ice jam shapes at these locations. The same was true for jams toed at km 1030. Additionally, ice jams toed at km 1070 and km 1080 produced similar peak flows and top of ice levels in the delta. To account for this non-linearity, a ranking system was developed and used in conjunction with the MLR analyses. The values of each of the five key variables were ranked in terms of how high the top of ice levels they generally produced in the delta (as indicated by the model results of the hypothetical events) and assigned a corresponding ranking value. For example, the toe location of km 1020 was given a rank of 2 and km 1030 a rank of 3, followed by km 1050 and km 1060 of 1 and 3, and km 1070 and km 1080 both of 4, km 1090 of 5 and km 1100 of 6. The complete ranking system is shown in Table 4.5. The simulated top of ice elevations from the hypothetical events were also ranked from low to high and mapped onto a 0 to 50 scale at each location. The range at each location is shown in Table 4.6. MLR equations were then developed between the total rank of the scenario and the ranks of the values of the key variables. The general form of the regression equation is shown below.

$$RS = b_1R_L + b_2R_T + b_3R_Q + b_4R_S + b_5R_{WL} + b_6 \quad (4-2)$$

where, RS is the total rank of the scenario predicted by the multiple linear regression equation; R_T and R_L are the ranks for the toe location and length of the upstream jam; R_Q is the rank for carrier

discharge; R_S is the rank for toe shift of the delta jam; R_{WL} is the rank for the lake level; b_j ($j = 1, 6$) are coefficients determined by multiple linear regression analysis. These new equations are summarized in Table 4.7, with the results of the equations shown in Figures 4.1-4.10b. The average error of the individual equations was reduced by 0.058 m on average, while the R^2 value at each location increased by 0.0162 on average.

Table 4.5 Rankings of the five key variables.

	Release Jam Length (L_j)		Release Jam Toe Location (T_j)		Carrier Discharge (Q_c)		Toe Shift (TS)		Downstream Lake level (LL)	
	(km)	Rank	(km)	Rank	(m ³ /s)	Rank	(km)	Rank	(m)	Rank
1	2.5	1	1020	2	200	1	0.55	1	156.6	1
2	5	2	1030	3	400	2	1.2	2	157.1	1.5
3	7.5	3	1050	1	600	3	1.4	3	157.6	2
4	10	4	1060	3	800	4	2.22	4	158.6	3
5	-	-	1070	4	1000	5	-	-	-	-
6	-	-	1080	4	1200	6	-	-	-	-
7	-	-	1090	5	-	-	-	-	-	-
8	-	-	1100	6	-	-	-	-	-	-

Table 4.6 Range of modelled top of ice elevations at key locations in the East Channel of the Hay River Delta.

Location (km)	1108.3	1109	1109.5	1109.98	1111	1111.55	1112.2	1112.36	1113.22	1113.61
Minimum Top of Ice (m)	160.2	159.9	159.5	158.9	158.1	156.9	156.6	156.6	156.63	156.6
Maximum Top of Ice (m)	168.3	167.3	166.7	165.9	164.9	164.3	164.0	163.9	161.46	159.2

Table 4.7 List of rankd MLR equations in the East Channel of the Hay River Delta.

Location (km)	Equation Criteria	b_1	b_2	b_3	b_4	b_5	b_6	Regression Error (m)
1108.3	$S_Q \leq 500 \text{ m}^3/\text{s}$	1.66	1.24	8.46	0.257	0.788	-12.4	0.235
	$S_Q = 501 - 900 \text{ m}^3/\text{s}$	2.51	1.94	5.2	0.175	0.866	-8.38	0.238
	$S_Q > 900 \text{ m}^3/\text{s}$	2.92	2.43	4.42	0.419	0.962	-8.12	0.251
1109	$S_Q \leq 500 \text{ m}^3/\text{s}$	1.63	1.2	8.29	0.309	0.81	-12.1	0.215
	$S_Q = 501 - 900 \text{ m}^3/\text{s}$	2.52	1.96	5.19	0.265	0.935	-9.04	0.232
	$S_Q > 900 \text{ m}^3/\text{s}$	2.96	2.47	4.57	0.514	0.974	-9.46	0.236
1109.5	$S_Q \leq 500 \text{ m}^3/\text{s}$	1.65	1.18	8.25	0.331	0.896	-12.2	0.205
	$S_Q = 501 - 900 \text{ m}^3/\text{s}$	2.54	1.95	5.16	0.295	1.02	-9.25	0.227
	$S_Q > 900 \text{ m}^3/\text{s}$	3.01	2.48	4.62	0.527	1.06	-10.1	0.231
1109.98	$S_Q \leq 500 \text{ m}^3/\text{s}$	1.67	1.15	8.15	0.115	1.16	-11.6	0.203
	$S_Q = 501 - 900 \text{ m}^3/\text{s}$	2.47	1.86	4.91	0.0064	1.16	-7.47	0.22
	$S_Q > 900 \text{ m}^3/\text{s}$	2.94	2.39	4.48	0.0985	1.13	-8.3	0.222
1111	$S_Q \leq 500 \text{ m}^3/\text{s}$	1.67	1.11	7.87	-0.394	1.04	-9.44	0.204
	$S_Q = 501 - 900 \text{ m}^3/\text{s}$	2.38	1.77	4.6	-0.764	1.19	-4.43	0.222
	$S_Q > 900 \text{ m}^3/\text{s}$	2.86	2.26	4.27	-0.527	1.28	-6.24	0.215

Table 4.7 List of ranked MLR equations in the East Channel of the Hay River Delta (continued).

Location (km)	Equation Criteria	b_1	b_2	b_3	b_4	b_5	b_6	Regression Error (m)
1111.55	$S_S = 0.55$ km	1.84	1.09	4.15	n/a	1.09	-5.79	0.426
	$S_S = 1.2$ km	2.16	1.61	5.32	n/a	0.487	-3.38	0.289
	$S_S = 1.4$ km	2.08	1.56	5.12	n/a	0.579	-3.46	0.272
	$S_S = 2.2$ km	2.18	1.67	5.28	n/a	0.905	-5.57	0.285
1112.2	$S_S = 0.55$ km	0.674	0.369	1.504	n/a	4.52	-6.32	0.208
	$S_S = 1.2$ km	1.63	1.05	3.24	n/a	3.43	-10	0.322
	$S_S = 1.4$ km	2.1	1.53	4.95	n/a	0.45	-5.52	0.282
	$S_S = 2.2$ km	2.25	1.78	5.59	n/a	0.673	-7.74	0.303
1112.36	$S_S = 0.55$ km	0.653	0.358	1.45	n/a	4.7	-7.07	0.195
	$S_S = 1.2$ km	0.877	0.725	2.24	n/a	5.61	-10.9	0.245
	$S_S = 1.4$ km	1.87	1.24	4.14	n/a	3.72	-11.6	0.334
	$S_S = 2.2$ km	2.3	1.82	5.72	n/a	0.668	-9.21	0.307
1113.22	$S_{WL} < 157.6$ m & $S_S < 2.2$ km	0.554	0.402	1.86	0.0054	7.19	-11.2	0.0787
	$S_{WL} \geq 157.6$ m & $S_S < 2.2$ km	0.871	0.725	1.83	1.64	7.14	-13.1	0.165
	$S_Q \leq 600$ m ³ /s & $S_S = 2.22$ km	1.48	0.874	4.14	n/a	10.1	-20.1	0.254
	$S_Q > 600$ m ³ /s & $S_S = 2.22$ km	2.82	2.26	4.97	n/a	5.57	-24.2	0.3
1113.61	$S_{WL} < 157.6$ m	0.573	0.43	1.88	0.0027	16.3	-20.6	0.045
	$S_{WL} \geq 157.6$ m	0.981	0.692	1.72	0.745	16.3	-20.9	0.085

4.3 Flood Level Prediction Tool

The rank based regression equations were used as the basis for the development of a flood level prediction tool for the East Channel of the delta. This tool uses the toe location and length of the upstream ice jam, the carrier discharge, and the downstream lake level as defined inputs. These values can be known well in advance of any delta flooding that may occur. The carrier discharge and lake level can be obtained from WSC or EMO gauge stations. Information on the upstream ice jam(s) can be obtained through aerial reconnaissance observations. As it is not possible to accurately predict the distance that the delta jams toe may shift downstream during consolidation triggered by the incoming release wave, the tool was configured to calculate four possible top of ice levels for each considered toe shift at each location in the East Channel. The maximum and minimum values at each location are then output. The sum of the modelling error as determined from the validation results and the average error of each regression equation was used to estimate the error bound at each location. The complete code of the prediction tool is shown in Appendix A.

The accuracy of the prediction tool was evaluated through comparison to two historical events (1992 and 2007) involving the consolidation of ice jams in the East Channel of the delta. The results were also compared to predictions by the IJPG developed by Brayall and Hicks (2012) using 2-D modelling. The 1992 event consisted of an estimated 5 km long jam releasing from km 1090 with a carrier discharge of $567 \text{ m}^3/\text{s}$, causing the consolidation of an ice jam in the delta with a downstream lake level of 157.04 m. The delta ice jam shifted to km 1112.6, resulting in significant flooding. Figure 4.11 shows the highest and lowest top of ice profiles calculated by the prediction tool resulting from different toe shifts. The predicted top of ice levels agree reasonably well with the surveyed top of ice profile, while also providing a much closer

representation of the observed profile than the IJPG results for the same jam. Additionally, the error bounds of the prediction tool are smaller than those of the IJPG, with the exception of locations where the IJPG calculated values of zero error, a result of the IJPG extrapolating the peak discharge of the modelled event, which fell outside the range of discharges the IJPG was developed with. The IJPG also incorrectly captured the top of ice levels of the downstream end of the reach as it interpolates the lake level based on ratings curves, rather than allowing the lake level of an event to be specified.

The 2007 event consisted of the release of a 4.8 km long jam toed at km 1025.9 with a carrier discharge of 290 m³/s. This release shifted an ice jam in the delta to km 1111.3 with a lake level of 158.62 m, triggering minor flooding in the downstream end of the delta. As the 2007 event did not have any surveyed top of ice values, comparisons were only made to the elevations of key landmarks within the delta that would denote flooding if exceeded. Figure 4.12 shows the predicted top of ice levels with error bounds below key landmark elevations through most of the East Channel excepting a region towards the downstream end. Therefore, the tool provides a reasonable estimate of flood conditions. The predicted top of ice levels from the IJPG were below the landmark elevations, excepting the upper error bound at km 1110.5, indicating the prediction tool provides a closer estimate of the flood conditions as compared to the IJPG. The error bounds were mostly comparative between the two tools except for km 1111 where the proposed tool has a much smaller error bound than IJPG.

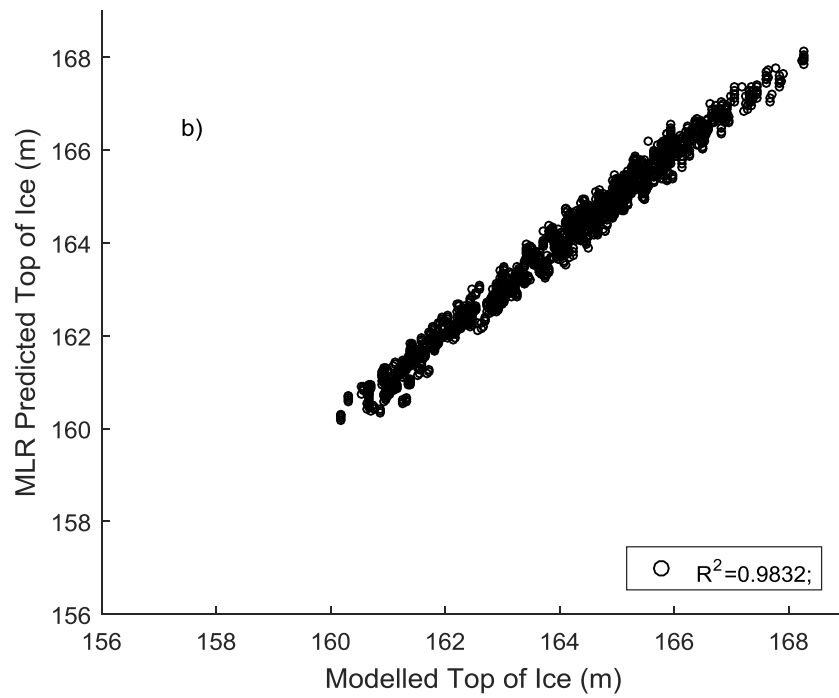
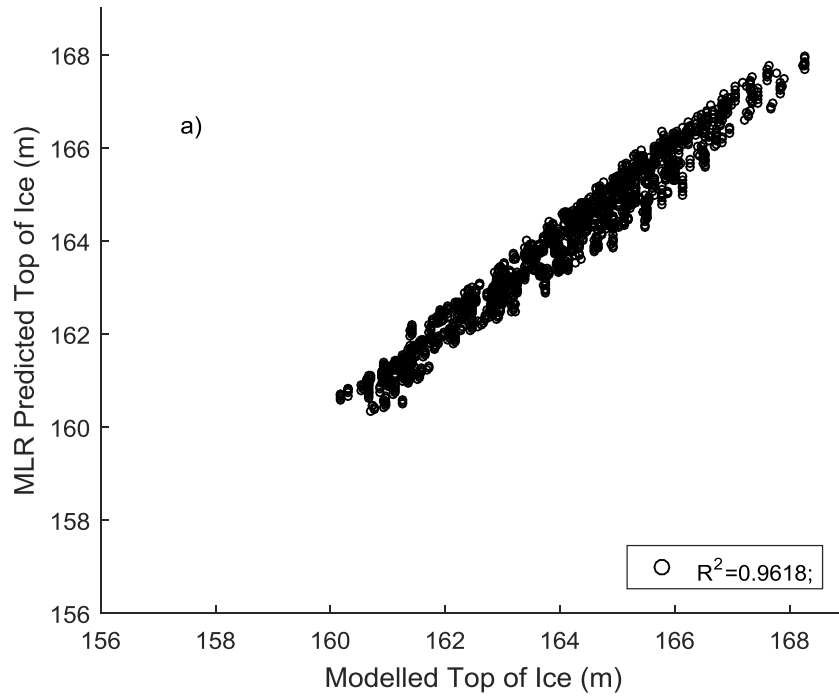


Figure 4.1 Comparison between the predicted and the simulated top of ice level at Km 1108.3 for the two regression methods: a) without rank and b) with rank.

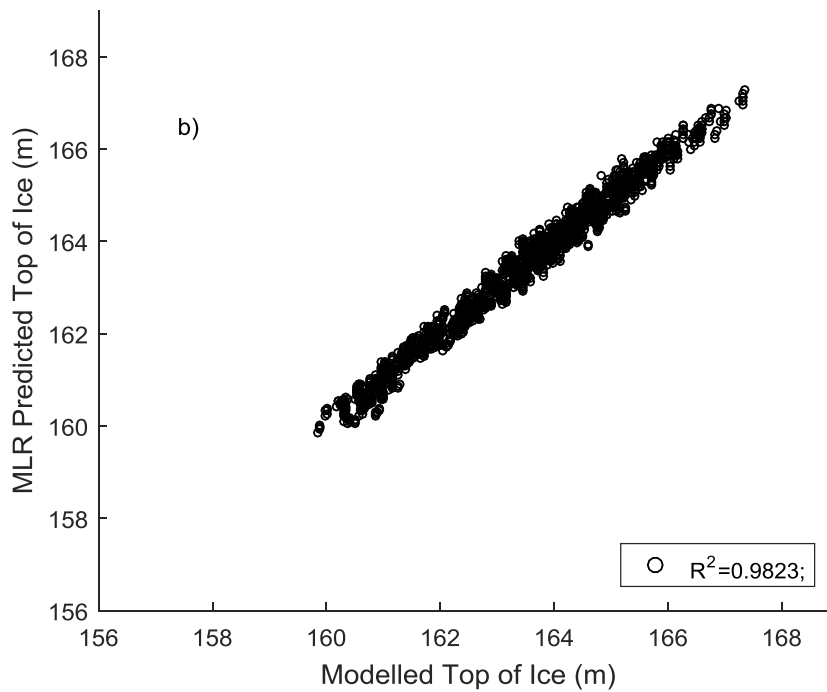
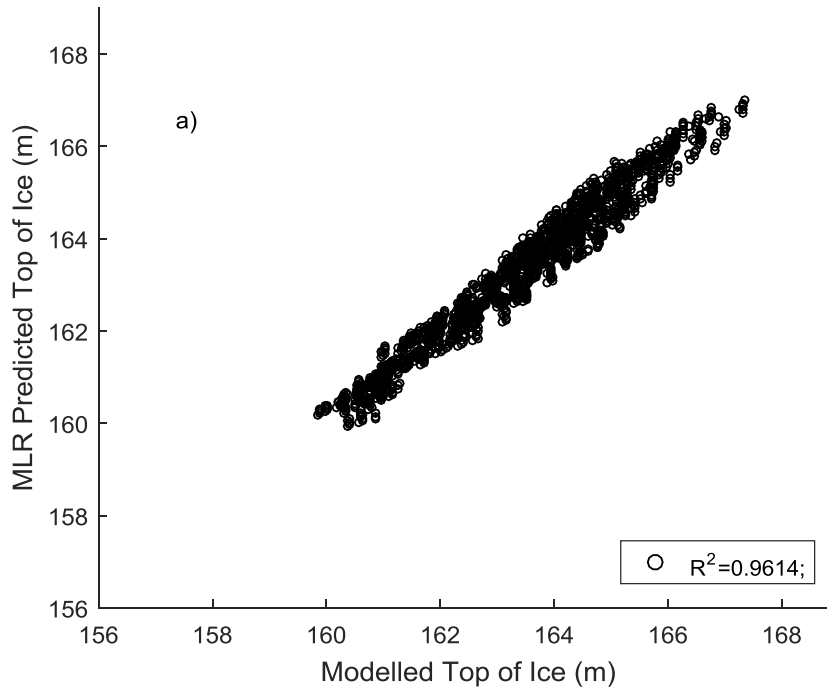


Figure 4.2 Comparison between the predicted and the simulated top of ice level at Km 1109 for the two regression methods: a) without rank and b) with rank.

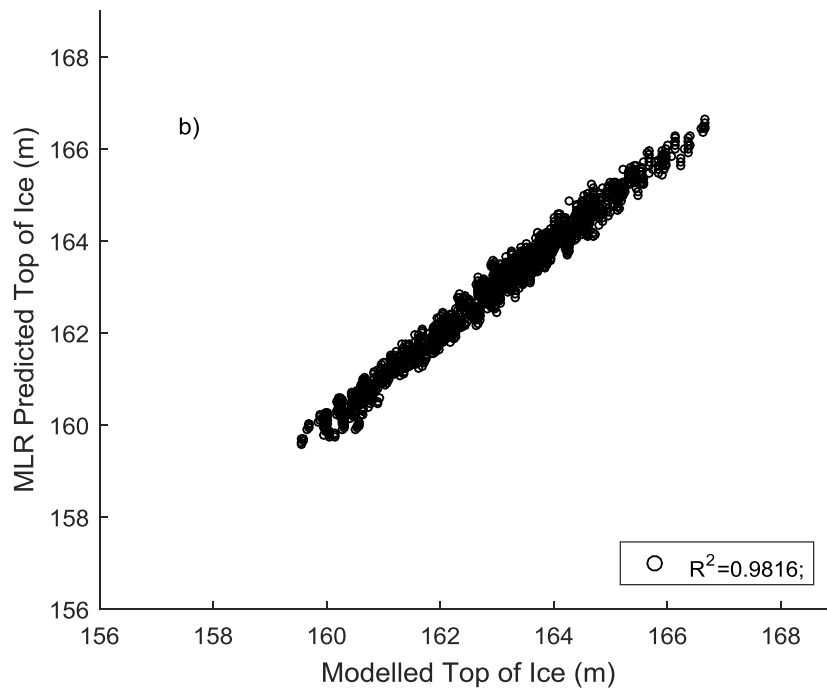
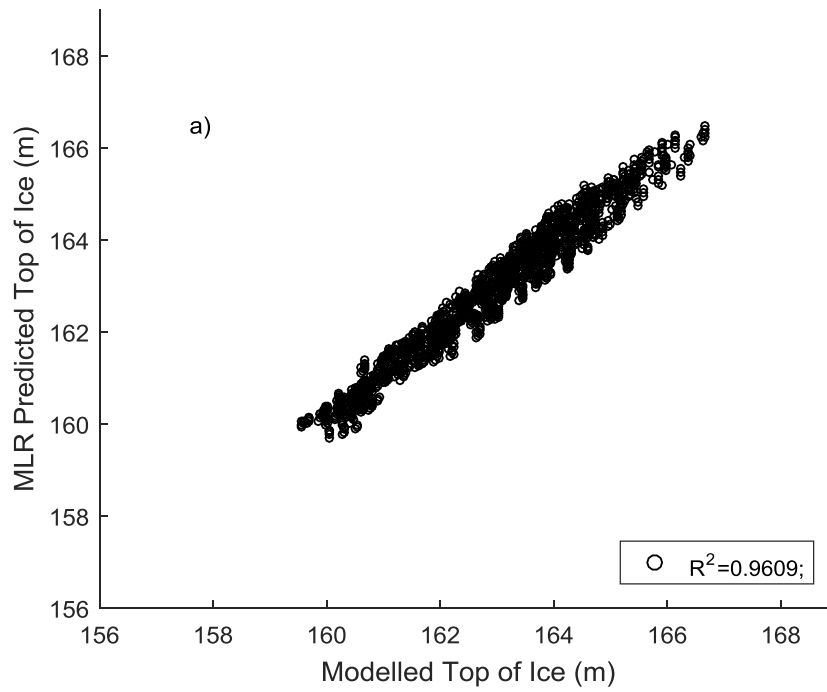


Figure 4.3 Comparison between the predicted and the simulated top of ice level at Km 1109.5 for the two regression methods: a) without rank and b) with rank.

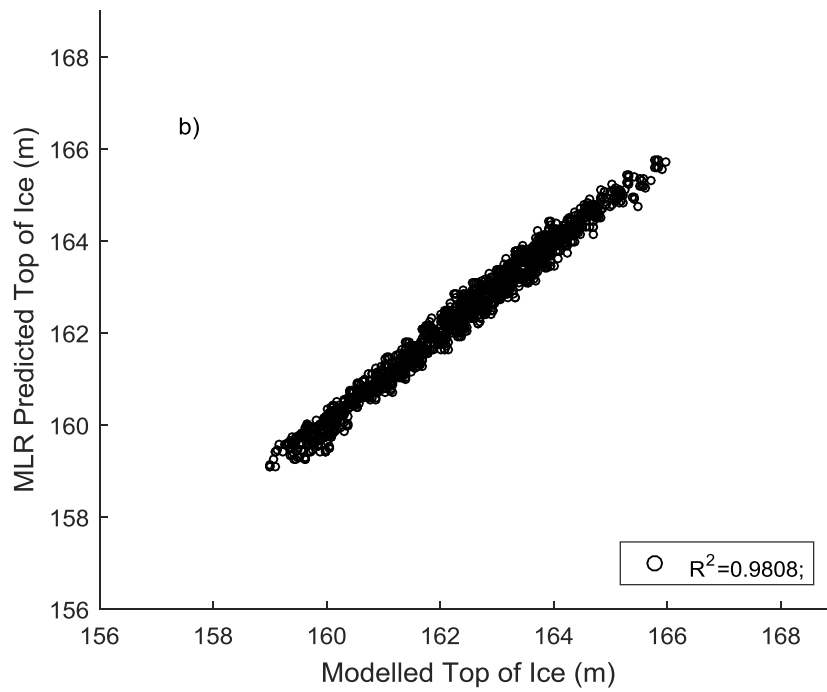
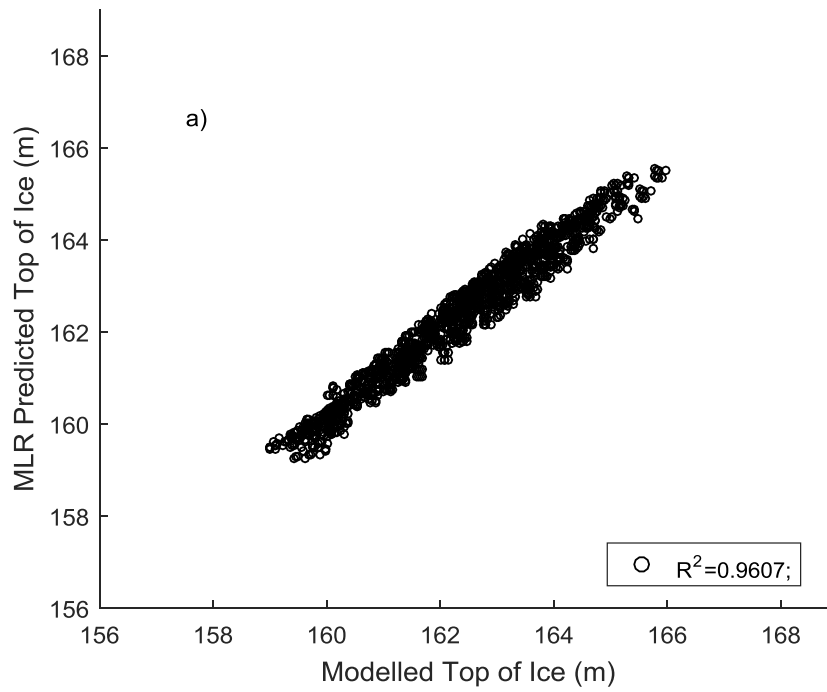


Figure 4.4 Comparison between the predicted and the simulated top of ice level at Km 1109.98

for the two regression methods: a) without rank and b) with rank.

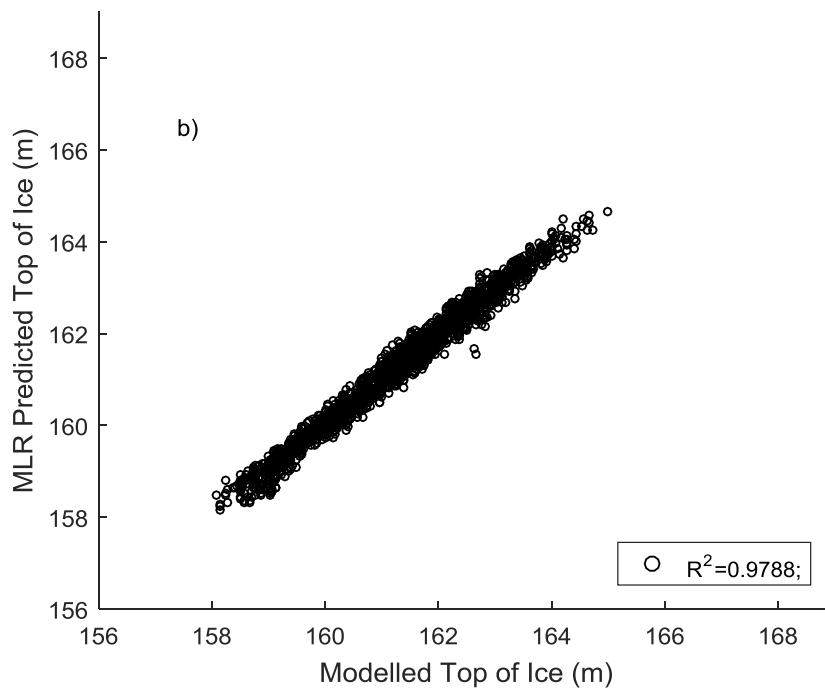
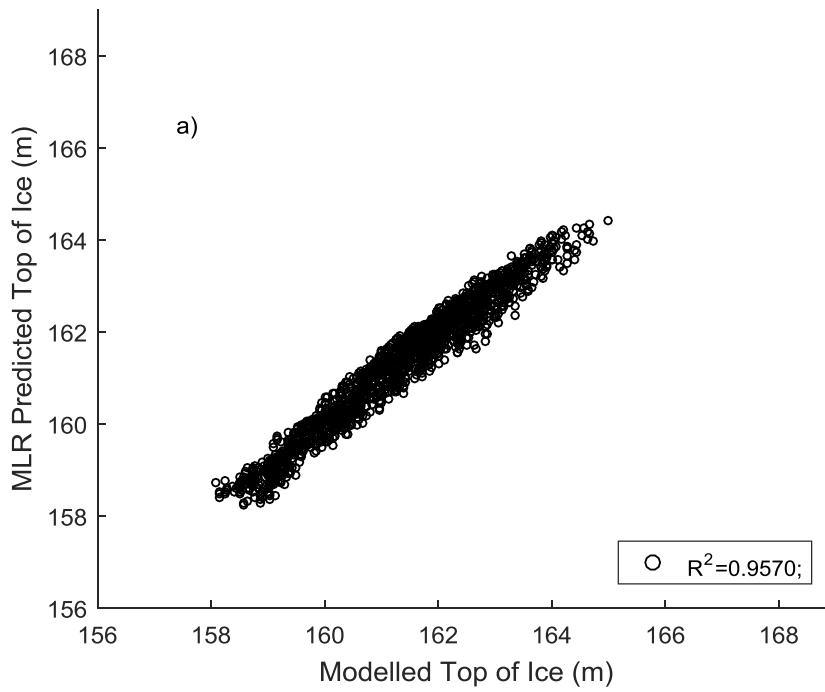


Figure 4.5 Comparison between the predicted and the simulated top of ice level at Km 1111 for the two regression methods: a) without rank and b) with rank.

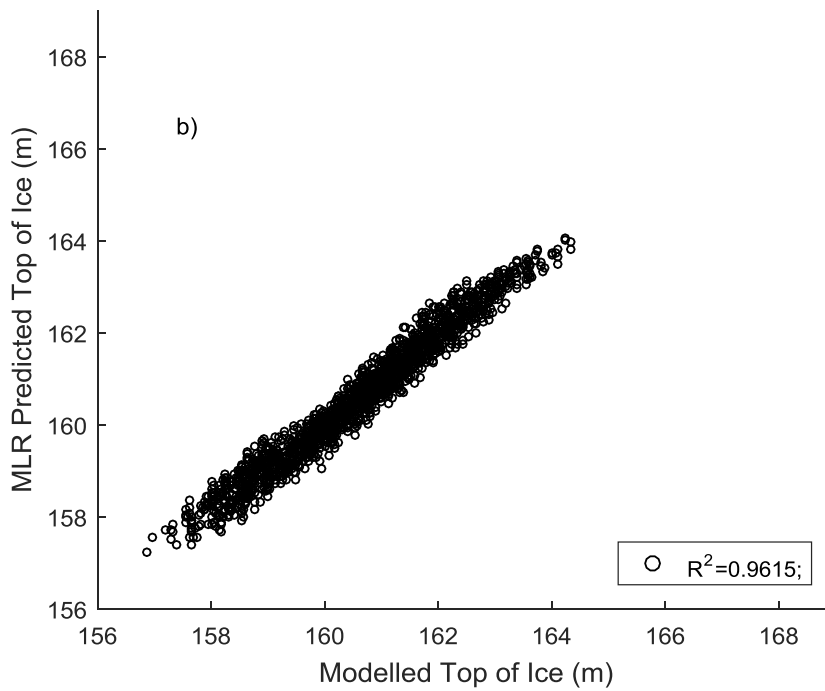
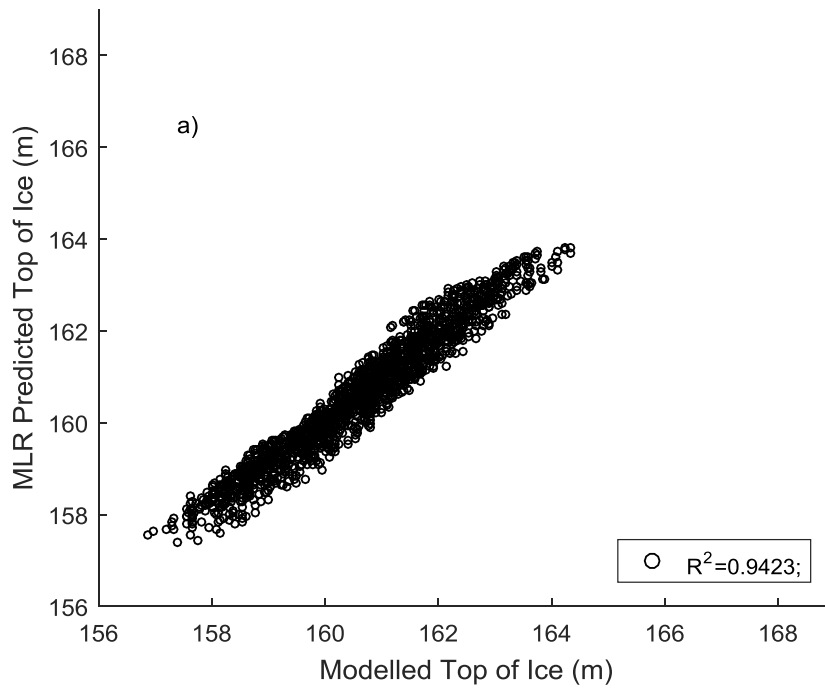


Figure 4.6 Comparison between the predicted and the simulated top of ice level at Km 1111.55

for the two regression methods: a) without rank and b) with rank.

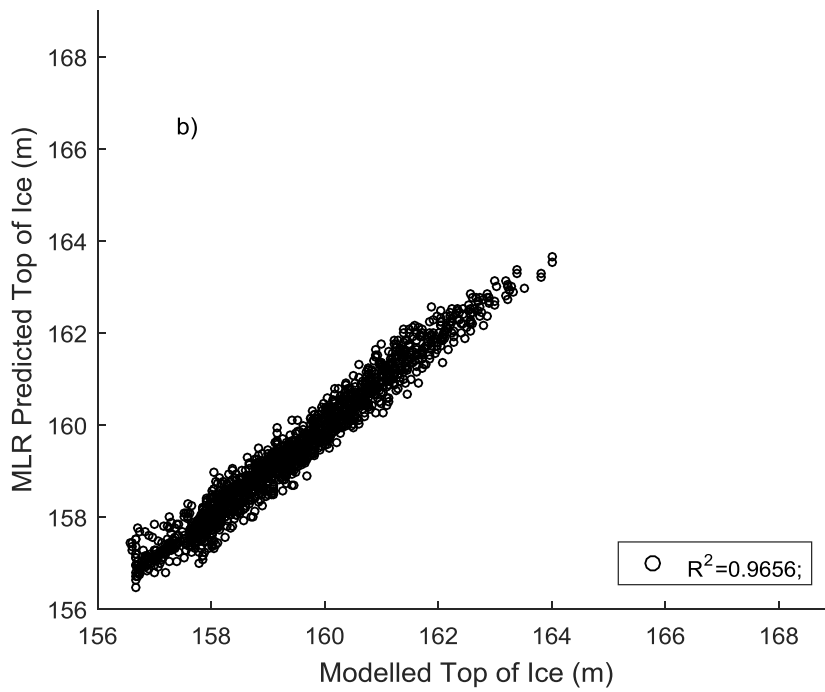
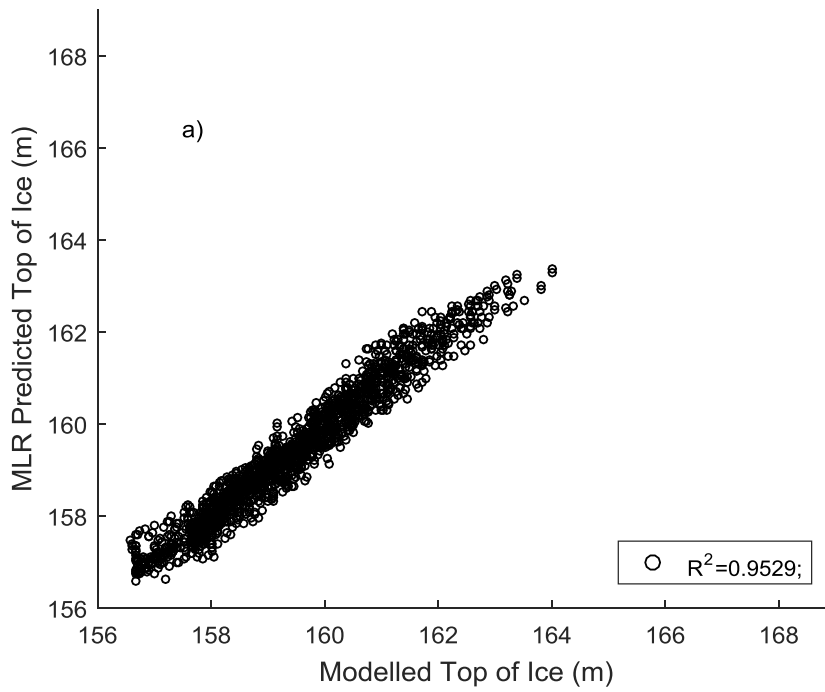


Figure 4.7 Comparison between the predicted and the simulated top of ice level at Km 1112.2 for the two regression methods: a) without rank and b) with rank.

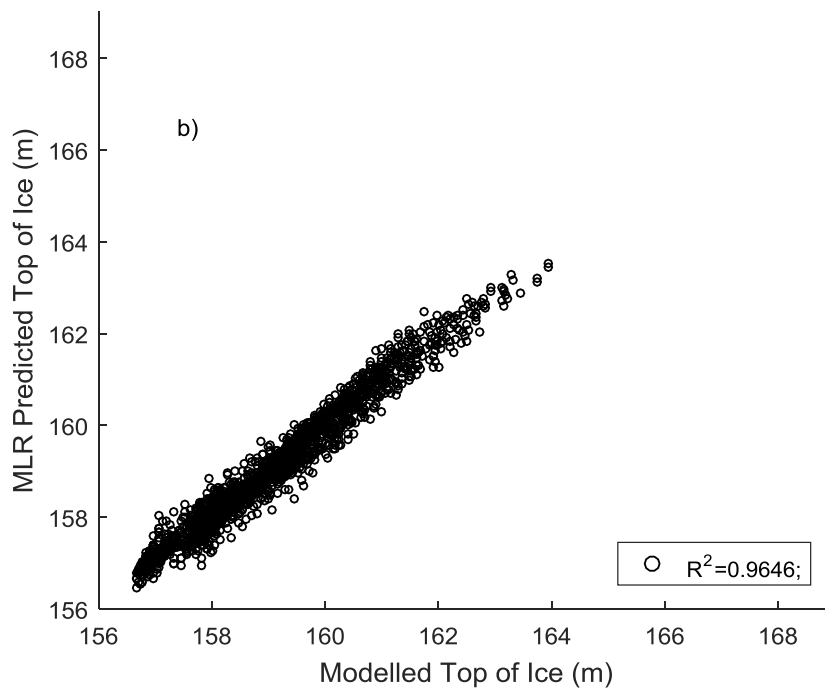
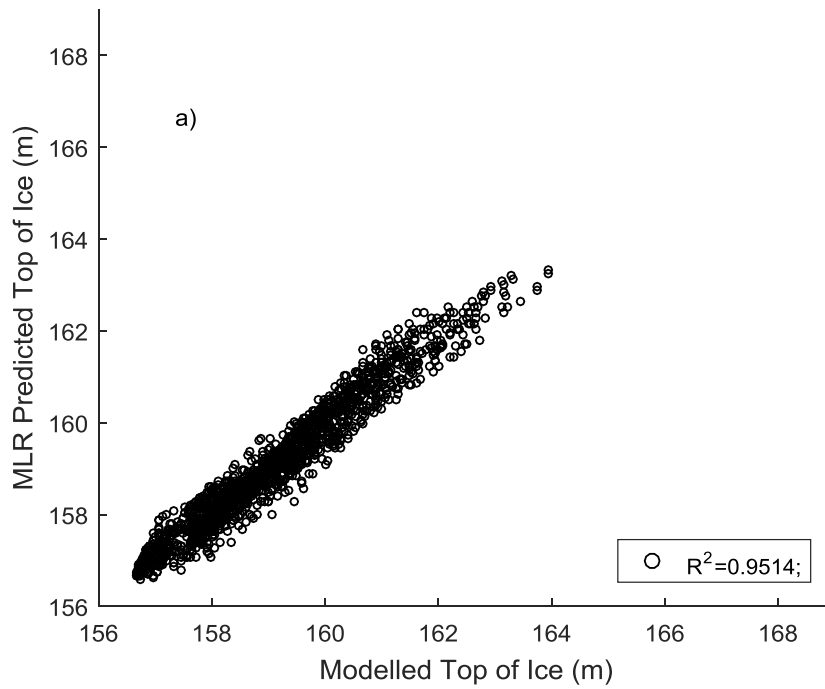


Figure 4.8 Comparison between the predicted and the simulated top of ice level at Km 1112.4 for the two regression methods: a) without rank and b) with rank.

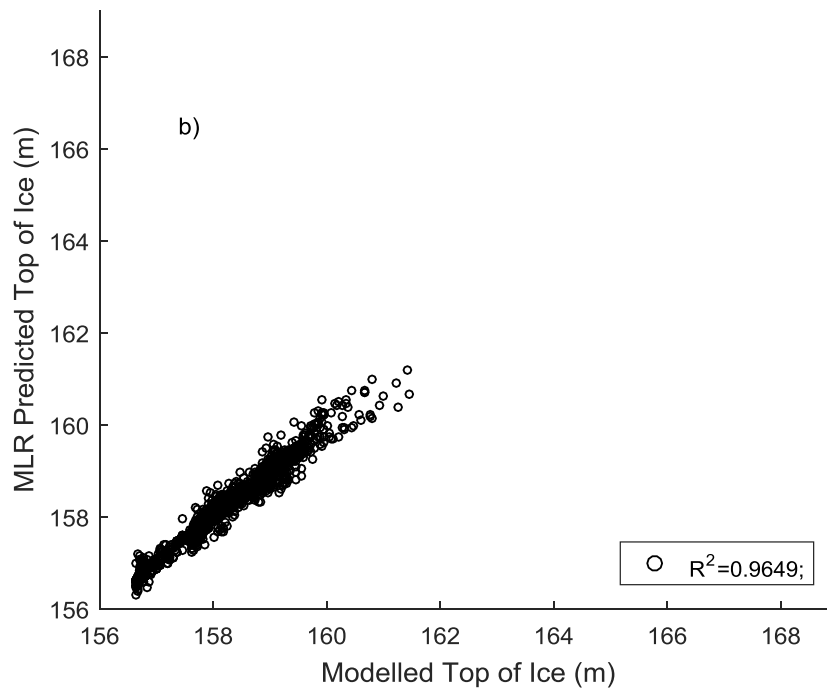
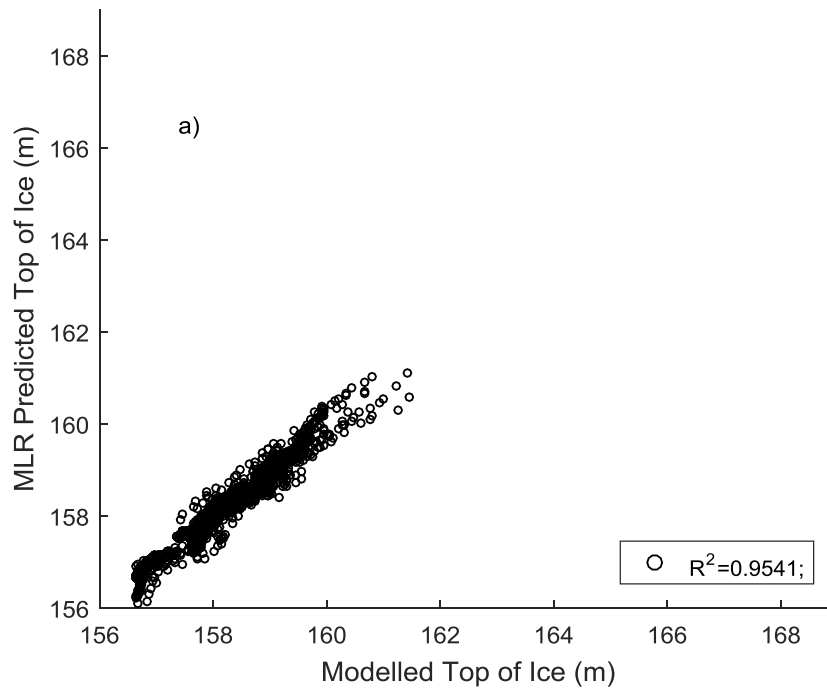


Figure 4.9 Comparison between the predicted and the simulated top of ice level at Km 1113.22

for the two regression methods: a) without rank and b) with rank.

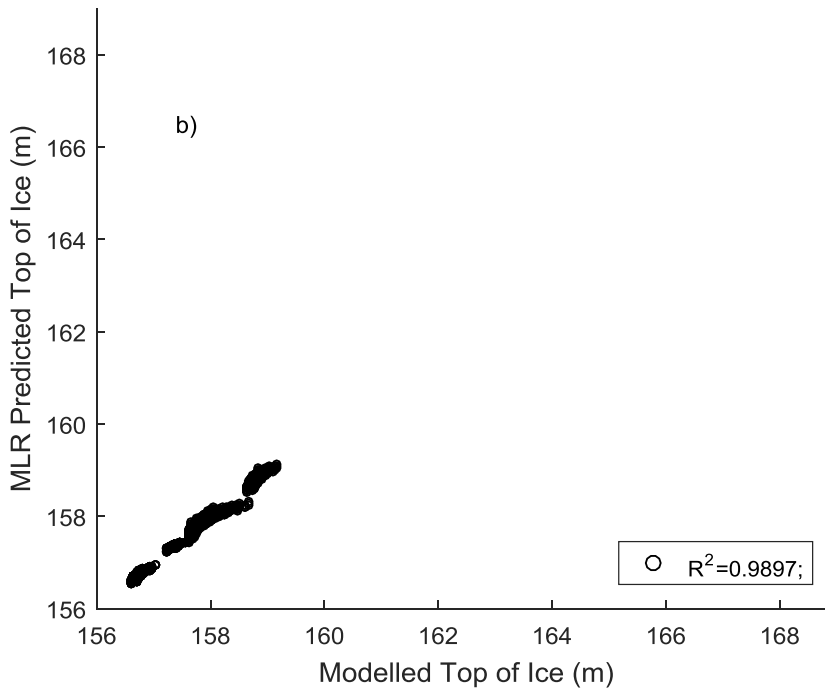
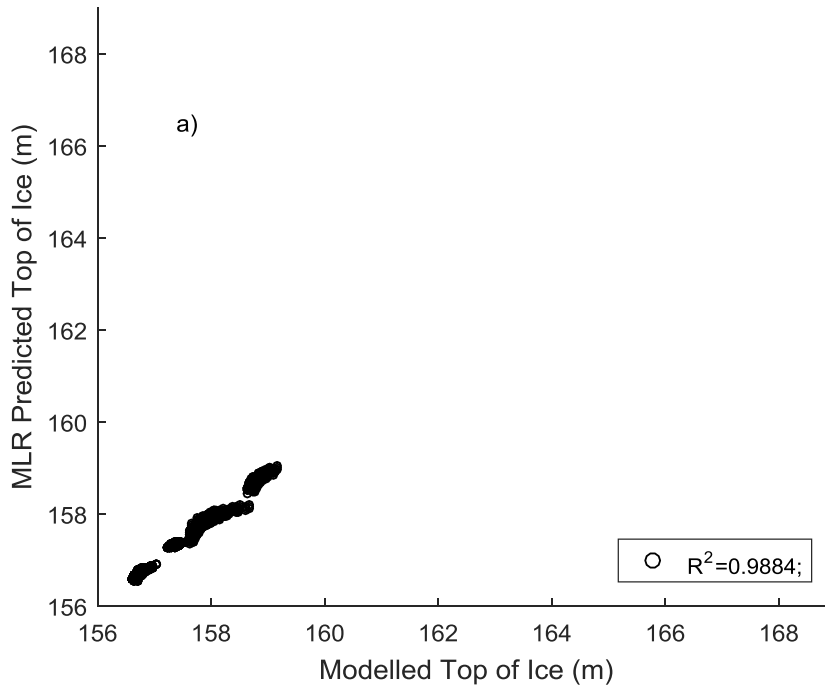


Figure 4.10 Comparison between the predicted and the simulated top of ice level at Km 1113.61

for the two regression methods: a) without rank and b) with rank.

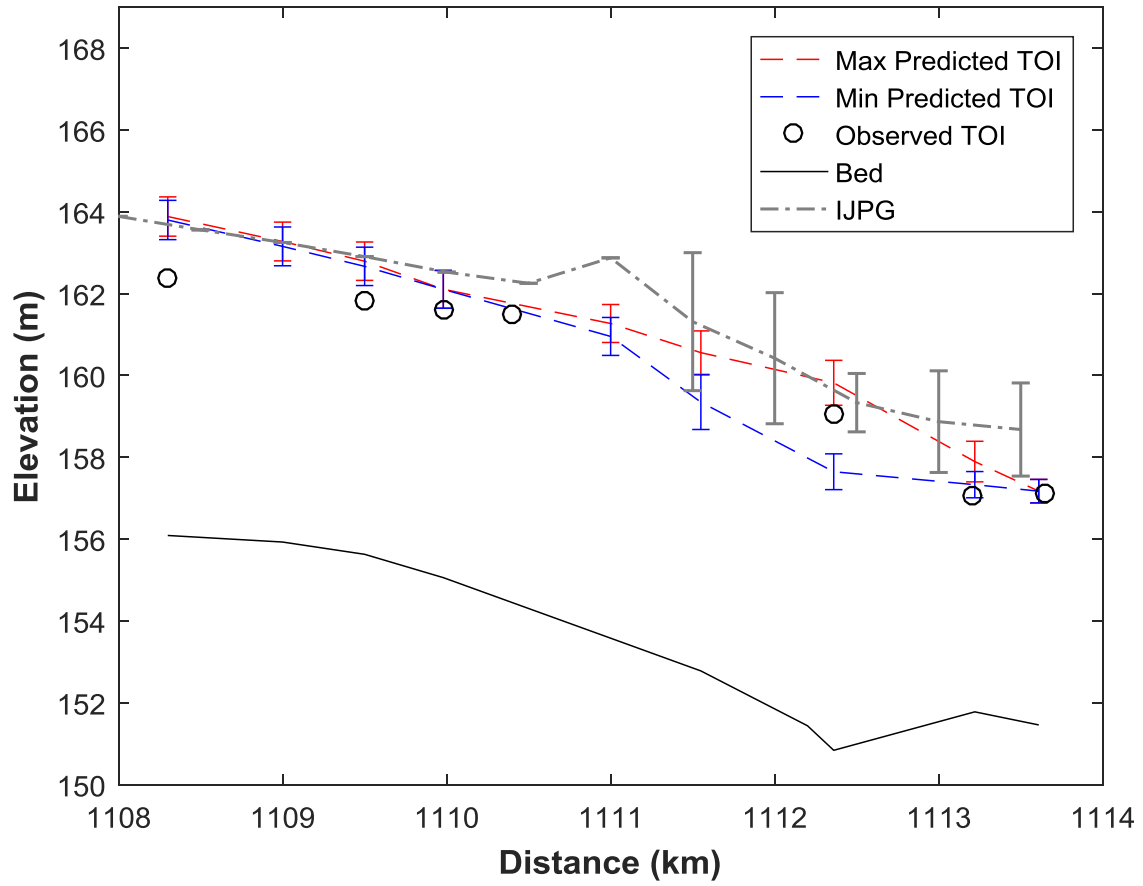


Figure 4.11 Comparison of the top of ice level predicted by the proposed tool, the IJPG and the observation for the 1992 flooding event.

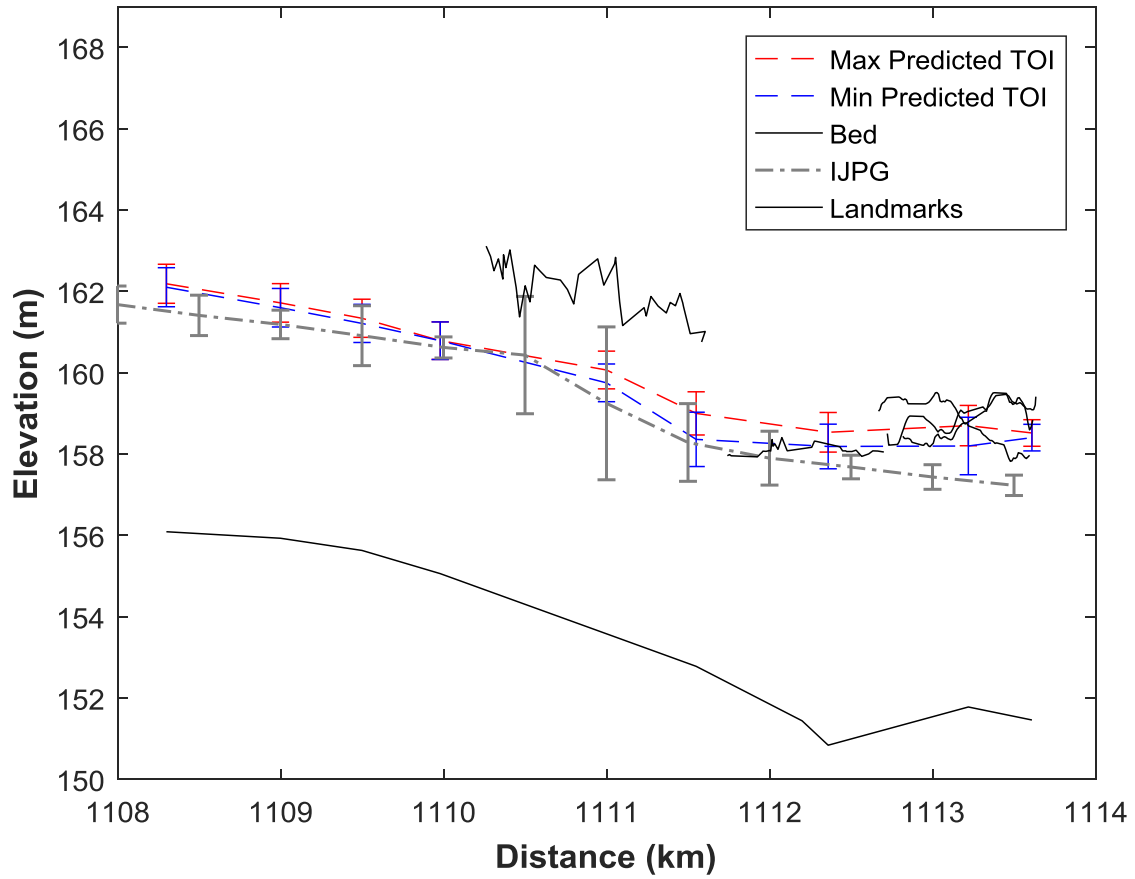


Figure 4.12 Comparison of the top of ice level predicted by the proposed tool, the IJPG and the key landmarks for the 2007 flooding event.

Chapter 5 : Summary and Conclusions

The release of ice jams in the upstream reaches of the Hay River has been identified as an important factor in the consolidation of ice jams within the Hay River Delta. The consolidation often leads to much thicker and longer ice jams, resulting in flooding in the delta region and presenting a threat to the Town of Hay River and other communities situated near or within the delta. The objective of this research was to develop an operational tool capable of predicting ice jam flood levels in the delta triggered by ice jam consolidation. This tool utilised a sequence of three 1-D models, the *RiverID* Ice Jam Release model, the *RiverID* Network model, and the *HEC-RAS* model, to simulate the upstream ice jam formation and release, the release wave propagating through the delta, and the top of ice profile of the consolidated ice jam in the delta. This new integrated modelling method was validated through comparison to breakup events occurred in 2008 and 2009 and was shown to produce plausible results when compared to the top of ice measurements taken during these events, with an average modelling error of 0.242 m.

The validated modelling method was then used to simulate a large quantity of hypothetical events, covering a variety of potential combinations of upstream and delta ice jam conditions. Simulated results from these events, specifically the top of ice levels output at key locations along the East Channel, were then analyzed using MLR analyses. The analyses produced a series of regression equations describing the relationship between the top of ice level at different locations along the East Channel and the five variables: carrier discharge, toe location of the upstream jam, length of the upstream jam, post-wave toe shift of the delta jam, and the downstream lake level. Two sets of regression equations were developed: one based on the original values and the other based on ranks of the top of ice levels and the key variables. It was shown that the regression equations with the ranking system provided a better prediction of

the simulated top of ice levels with an average reduction of error of 0.058 m and an average increase of the R^2 value of 0.0162 on average. These equations also demonstrated the sensitivity of top of ice levels in the delta to the different variables. Upstream locations were sensitive to carrier discharge, locations in the toe shift region were sensitive to the distance of the toe shift, and locations in the downstream end of the channel were sensitive to the lake level.

The regression equations obtained with the ranking system were used in the development of a flood level prediction tool for the Town of Hay River. The tool uses information that can be available well in advance of any delta flooding as input, producing top of ice profiles for the East Channel of the delta. A range of possible delta jam toe shifts were considered, allowing the effects of jam toe shifting during the consolidation event in the delta to be explicitly accounted for. The accuracy of the tool was compared both to surveyed top of ice levels, documented flood severity and the results of the previously developed IJPG for two historical events. In both cases, the results of the proposed prediction tool compared well with the historical events, and provided improved accuracy and smaller amounts of error in comparison to the results obtained from 2-D modelling.

The same method as described in this study can be applied to the West Channel for a complete coverage of flood forecasting for the Hay River Delta. This research also demonstrated the viability of using 1-D models in simulating ice jam release and subsequent ice jam consolidation in complex multi-channel networks. Comparable accuracy with 2-D modelling was achieved yet with much lesser data requirements and modelling efforts. Therefore, further work is recommended for the development of an integrated 1-D network model which is capable of predicting ice jam caused flooding in complex multi-channel network systems similar to the Hay River Delta.

References

- Blackburn, J., She, Y., Hicks, F., and Nafziger, J., 2015. Ice effects on flow distributions in the Mackenzie Delta. *In Proceedings of 18th Workshop on the Hydraulics of Ice Covered Rivers*, Quebec City, Quebec, 18-20 August, 2015.
- Brayall, M., 2011. 2-D hydraulic and ice process modeling at Hay River, NWT. MSc. Thesis, Department of Civil Engineering, University of Alberta, Edmonton, AB
- Brayall, M., and Hicks, F., 2012. Applicability of 2-D modeling for forecasting ice jam flood levels in the Hay River Delta, Canada. *Canadian Journal of Civil Engineering*, **39**:701-712
- Flato, G., and Gerard, R., 1986. Calculation of ice jam thickness profiles. *In Proceedings of 4th Workshop on Hydraulics of River Ice*, Subcommittee of Hydraulics of Ice Covered Rivers, National Research Council of Canada, Montreal, 19-20 June, 1986.
- Gerard, R., and Stanley, S., 1988. Ice jams and flood forecasting, Hay River, N.W.T. Environment Canada and Indian and Northern Affairs Canada, Yellowknife, N.W.T.
- Gerard, R., Hicks, F., and Jasek, M., 1990. Ice jams and flood forecasting, Hay River, N.W.T.- Phase 2: Surges and interactive computer program development. Environment Canada and Indian and Northern Affairs Canada, Yellowknife, N.W.T.
- Hicks, F.E., Steffler, P.M. and Gerard, R., 1992. Finite Element Modeling of Surge Propagation and an Application to the Hay River, NWT, *Canadian Journal of Civil Engineering*, **19**(3): 454-462.

Kovachis, N. Hicks, F., Zhao, L. and Maxwell, J. 2010. Development of an expert system for forecasting the progression of breakup at Hay River, NWT, Canada. *In* Proceedings of 20th IAHR Ice Symposium, Lahti, Finland, 14-18 June, 2010.

Kovachis, N., 2011. Patterns of river breakup timing and sequencing, Hay River, NWT. MSc. Thesis, Department of Civil Engineering, University of Alberta, Edmonton, AB

Pariset, E., Hausser, R. and Gagon, A., 1966. Formation of ice covers and ice jams in rivers. *Journal of Hydraulics Division, Proc. of the American Society of Civil Engineers*, **92**(HY6): 1-23.

She, Y. and F. Hicks 2005. Incorporating ice effects in ice jam release surge models. *In* Proceedings of 13th Workshop on River Ice, Hanover, NH, 16-18 Sept. 2005, CGU-HS CRIPE, pp. 470-484.

She, Y. and Hicks, F., 2006. Modelling ice jam release waves with consideration for ice effects. *Cold Regions Science and Technology*, **45**:137-147.

She, Y., Hicks, F., Steffler, P. and Healy, D., 2008. Effects of unsteadiness and ice motion on river ice jam profiles. *In* Proceedings of 19th IAHR International Symposium on Ice, Vancouver, British Columbia, 6-11 July, 2008.

Uzuner, M.S. and J.F. Kennedy 1976. Theoretical model of river ice jams. *ASCE Journal of Hydraulic Engineering*, **102**(9): 1365-1383.

Watson, D., Hicks, F., and Andrishak, R., 2009. Analysis of observed 2008 ice jam release events on the Hay River, NWT. *In* Proceedings of 15th Workshop on River Ice, St John's,

Newfoundland, 15-17 June, 2009. CGU HS Committee on River Ice Processes and the Environment.

Watson, D., 2011. Observation and modeling of ice jam release events on the Hay River, NWT. MSc. Thesis, Department of Civil Engineering, University of Alberta, Edmonton, AB

Zhao, L., 2012. River ice breakup forecasting using artificial neural networks and fuzzy logic systems. MSc thesis, Department of Civil Engineering, University of Alberta, Edmonton, AB.

Appendix A: Matlab Code of the Flood Level Prediction Tool

```

clc;
clear;
importfile('Data Analysis');

%User Defined Scenario Input
Length=4.8;
Toe=1025.9;
Flow=290;
Lake=158.62;

%Conversion of Scenario to rank
L=Length/2.5;
if Toe<=1030
    T=2;
elseif Toe>=1050 && Toe<1060
    T=(Toe-1050)/5+1;
elseif Toe>=1060 && Toe<1070
    T=(Toe-1060)/10+3;
elseif Toe>=1070 && Toe<1080
    T=4;
elseif Toe>=1080
    T=(Toe-1080)/10+4;
end
F=Flow/200;
l=Lake-155.6;
n=1

for j=1:4
    rank(j,1)=L;
    rank(j,2)=T;
    rank(j,3)=F;
    rank(j,4)=j;
    rank(j,5)=1;
end

%Calculation of top of ice values for km 1108.3
for k=1:4
    if input(1,3)<= 500
        sumrankA(k,1)=-12.4 +1.66*rank(k,1) +1.24*rank(k,2)
+8.46*rank(k,3)+.257*rank(k,4)+.788*rank(k,5);
        sumrankA(k,4)=.235
    elseif input(1,3)>= 901
        sumrankA(k,1)=-8.12 +2.92*rank(k,1) +2.43*rank(k,2)
+4.42*rank(k,3)+.419*rank(k,4)+.962*rank(k,5);
        sumrankA(k,4)=.251
    else
        sumrankA(k,1)=-8.38 +2.51*rank(k,1) +1.94*rank(k,2)
+5.2*rank(k,3)+.175*rank(k,4)+.866*rank(k,5);
        sumrankA(k,4)=.238
    end
    sumrankA(k,2)=1108.3;
    sumrankA(k,3)=(sumrankA(k,1)/50)*(168.26-160.16)+160.16;
end

```

```

graphrank(1,1)=max(sumrankA(:,3));
graphrank(1,2)=min(sumrankA(:,3));
graphrank(1,3)=sumrankA(1,4);
graphrank(1,4)=sumrankA(1,4);

%Calculation of top of ice values for km 1109
for k=1:4
    if input(1,3)<= 500
        sumrankB(k,1)=-12.1+1.63*rank(k,1)+1.2*rank(k,2)+8.29*rank(k,3)
+.309*rank(k,4)+.81*rank(k,5);
        sumrankB(k,4)=.215
    elseif input(1,3)>= 901
        sumrankB(k,1)=-9.46+2.96*rank(k,1)+2.47*rank(k,2)+4.57*rank(k,3)
+.514*rank(k,4)+.974*rank(k,5);
        sumrankB(k,4)=.236
    else
        sumrankB(k,1)=-9.04+2.52*rank(k,1)+1.96*rank(k,2)+5.19*rank(k,3)
+.265*rank(k,4)+.935*rank(k,5);
        sumrankB(k,4)=.232
    end
    sumrankB(k,2)=1109;
    sumrankB(k,3)=(sumrankB(k,1)/50)*(167.333-159.85)+159.85;
end

graphrank(2,1)=max(sumrankB(:,3));
graphrank(2,2)=min(sumrankB(:,3));
graphrank(2,3)=sumrankB(1,4);
graphrank(2,4)=sumrankB(1,4);

%Calculation of top of ice values for km 1109.5
for k=1:4
    if input(n,3)<= 500
        sumrankC(k,1)=-12.2+1.65*rank(k,1)+1.18*rank(k,2)+8.25*rank(k,3)
+.331*rank(k,4)+.896*rank(k,5);
        sumrankC(k,4)=.205
    elseif input(n,3)>= 901
        sumrankC(k,1)=-10.1+3.01*rank(k,1)+2.48*rank(k,2)+4.62*rank(k,3)
+.527*rank(k,4)+1.06*rank(k,5);
        sumrankC(k,4)=.231
    else
        sumrankC(k,1)=-9.25+2.54*rank(k,1)+1.95*rank(k,2)+5.16*rank(k,3)
+.295*rank(k,4)+1.02*rank(k,5);
        sumrankC(k,4)=.227
    end
    sumrankC(k,2)=1109.5;
    sumrankC(k,3)=(sumrankC(k,1)/50)*(166.67-159.54)+159.54;
end

graphrank(3,1)=max(sumrankC(:,3));
graphrank(3,2)=min(sumrankC(:,3));
graphrank(3,3)=sumrankC(1,4);
graphrank(3,4)=sumrankC(1,4);

```

```

%Calculation of top of ice values for km 1109.98
for k=1:4
    if input(n,3)<= 500
        sumrankD(k,1)=-11.6+1.67*rank(k,1)+1.15*rank(k,2)+8.15*rank(k,3)
+.115*rank(k,4)+1.16*rank(k,5);
        sumrankD(k,4)=.203
    elseif input(n,3)>= 901
        sumrankD(k,1)=-8.3+2.94*rank(k,1)+2.39*rank(k,2)+4.48*rank(k,3)
+.0985*rank(k,4)+1.13*rank(k,5);
        sumrankD(k,4)=.222
    else
        sumrankD(k,1)=-7.47+2.47*rank(k,1)+1.86*rank(k,2)+4.91*rank(k,3)
+.0064*rank(k,4)+1.16*rank(k,5);
        sumrankD(k,4)=.22
    end
    sumrankD(k,2)=1109.98;
    sumrankD(k,3)=(sumrankD(k,1)/50)*(165.98-158.98)+158.98;
end

graphrank(4,1)=max(sumrankD(:,3));
graphrank(4,2)=min(sumrankD(:,3));
graphrank(4,3)=sumrankD(1,4);
graphrank(4,4)=sumrankD(1,4);

%Calculation of top of ice values for km 111
for k=1:4
    if input(n,3)<= 500
        sumrankE(k,1)=-9.44+1.67*rank(k,1) +1.11*rank(k,2) +7.87*rank(k,3) -
.394*rank(k,4) +1.04*rank(k,5);
        sumrankE(k,4)=.204
    elseif input(n,3)>= 901
        sumrankE(k,1)=-6.24+2.86*rank(k,1)+2.26*rank(k,2) +4.27*rank(k,3) -
.527*rank(k,4)+1.28*rank(k,5);
        sumrankE(k,4)=.215
    else
        sumrankE(k,1)=-4.43+2.38*rank(k,1)+1.77*rank(k,2) +4.6*rank(k,3) -
.764*rank(k,4)+1.19*rank(k,5);
        sumrankE(k,4)=.222
    end
    sumrankE(k,2)=1111;
    sumrankE(k,3)=(sumrankE(k,1)/50)*(164.98-158.08)+158.08;
end

graphrank(5,1)=max(sumrankE(:,3));
graphrank(5,2)=min(sumrankE(:,3));
graphrank(5,3)=sumrankE(1,4);
graphrank(5,4)=sumrankE(1,4);

```

```

%Calculation of top of ice values for km 1111.55
for k=1:4
    if rank(k,4)== 1
        sumrankF(k,1)=-5.79+1.84*rank(k,1)+1.09*rank(k,2)
+4.15*rank(k,3)+1.09*rank(k,5);
        sumrankF(k,4)=.426
    elseif rank(k,4)== 2
        sumrankF(k,1)=-3.38+2.16*rank(k,1)+1.61*rank(k,2)
+5.32*rank(k,3)+.487*rank(k,5);
        sumrankF(k,4)=.289
    elseif rank(k,4)==3
        sumrankF(k,1)=-3.46+2.08*rank(k,1)+1.56*rank(k,2)
+5.12*rank(k,3)+.579*rank(k,5);
        sumrankF(k,4)=.272
    else
        sumrankF(k,1)=-5.57+2.18*rank(k,1)+1.67*rank(k,2)
+5.28*rank(k,3)+.905*rank(k,5);
        sumrankF(k,4)=.285
    end
    sumrankF(k,2)=1111.55;
    sumrankF(k,3)=(sumrankF(k,1)/50)*(164.32-156.87)+156.87;
end

graphrank(6,1)=max(sumrankF(:,3));
graphrank(6,2)=min(sumrankF(:,3));

for k=1:4
    if graphrank(6,1)==sumrankF(k,3)
        graphrank(6,3)=sumrankF(k,4);
    end

    if graphrank(6,2)==sumrankF(k,3)
        graphrank(6,4)=sumrankF(k,4);
    end
end
end

```

```

%Calculation of top of ice values for km 1112.2
for k=1:4
    if rank(k,4)== 1
        sumrankG(k,1)=-6.32+.674*rank(k,1)+.369*rank(k,2)
+1.504*rank(k,3)+4.52*rank(k,5);
        sumrankG(k,4)=.208
    elseif rank(k,4)== 2
        sumrankG(k,1)=-10+1.63*rank(k,1)+1.05*rank(k,2)
+3.24*rank(k,3)+3.43*rank(k,5);
        sumrankG(k,4)=.322
    elseif rank(k,4)==3
        sumrankG(k,1)=-5.52+2.1*rank(k,1)+1.53*rank(k,2)
+4.95*rank(k,3)+.45*rank(k,5);
        sumrankG(k,4)=.282
    else
        sumrankG(k,1)=-7.74+2.25*rank(k,1)+1.78*rank(k,2)
+5.59*rank(k,3)+.673*rank(k,5);
        sumrankG(k,4)=.303
    end
    sumrankG(k,2)=1112.2;
    sumrankG(k,3)=(sumrankG(k,1)/50)*(164.01-156.58)+156.58;
end

graphrank(7,1)=max(sumrankG(:,3));
graphrank(7,2)=min(sumrankG(:,3));

for k=1:4
    if graphrank(7,1)==sumrankG(k,3)
        graphrank(7,3)=sumrankG(k,4);
    end

    if graphrank(7,2)==sumrankG(k,3)
        graphrank(7,4)=sumrankG(k,4);
    end
end
end

```

```

%Calculation of top of ice values for km 1112.36
for k=1:4
    if rank(k,4)== 1
        sumrankh(k,1)=-7.07+.653*rank(k,1)+.358*rank(k,2)
+1.45*rank(k,3)+4.7*rank(k,5);
        sumrankh(k,4)=.195
    elseif rank(k,4)== 2
        sumrankh(k,1)=-10.9+.877*rank(k,1)+.725*rank(k,2)
+2.24*rank(k,3)+5.61*rank(k,5);
        sumrankh(k,4)=.245
    elseif rank(k,4)==3
        sumrankh(k,1)=-11.6+1.87*rank(k,1)+1.24*rank(k,2)
+4.14*rank(k,3)+3.72*rank(k,5);
        sumrankh(k,4)=.334
    else
        sumrankh(k,1)=-9.21+2.3*rank(k,1)+1.82*rank(k,2)
+5.72*rank(k,3)+.668*rank(k,5);
        sumrankh(k,4)=.307
    end
    sumrankh(k,2)=1112.36;
    sumrankh(k,3)=(sumrankh(k,1)/50)*(163.95-156.67)+156.67;
end

graphrank(8,1)=max(sumrankh(:,3));
graphrank(8,2)=min(sumrankh(:,3));

for k=1:4
    if graphrank(8,1)==sumrankh(k,3)
        graphrank(8,3)=sumrankh(k,4);
    end

    if graphrank(8,2)==sumrankh(k,3)
        graphrank(8,4)=sumrankh(k,4);
    end
end
end

```

```

%Calculation of top of ice values for km 1113.22
for k=1:4
    if rank(k,4)<4 && rank(k,5)< 2
        sumranki(k,1)=-11.2+.554*rank(k,1)+.402*rank(k,2) +1.86*rank(k,3)
+.0054*rank(k,4)+7.19*rank(k,5);
        sumranki(k,4)=.0787
    elseif rank(k,4)<4 && rank(k,5)>= 2
        sumranki(k,1)=-13.1+.871*rank(k,1)+.725*rank(k,2) +1.83*rank(k,3)
+1.64*rank(k,4)+7.14*rank(k,5);
        sumranki(k,4)=.465
    elseif rank(k,4)==4 && rank(k,3)<=3
        sumranki(k,1)=-20.1+1.48*rank(k,1)+.874*rank(k,2) +4.14*rank(k,3)
+10.1*rank(k,5);
        sumranki(k,4)=.254
    else
        sumranki(k,1)=-24.2+2.82*rank(k,1)+2.26*rank(k,2) +4.97*rank(k,3)
+5.57*rank(k,5);
        sumranki(k,4)=.3
    end
    sumranki(k,2)=1113.22;
    sumranki(k,3)=(sumranki(k,1)/50)*(161.46-156.63)+156.63
end

graphrank(9,1)=max(sumranki(:,3));
graphrank(9,2)=min(sumranki(:,3));

for k=1:4
    if graphrank(9,1)==sumranki(k,3)
        graphrank(9,3)=sumranki(k,4);
    end

    if graphrank(9,2)==sumranki(k,3)
        graphrank(9,4)=sumranki(k,4);
    end
end
end

```

```

%Calculation of top of ice values for km 1113.61
for k=1:4
    if rank(k,5)< 2
        sumrankj(k,1)=-20.6+.573*rank(k,1)+.43*rank(k,2)+1.88*rank(k,3)
+.0027*rank(k,4)+16.3*rank(k,5);
        sumrankj(k,4)=.045;
    else
        sumrankj(k,1)=-20.9+.981*rank(k,1)+.692*rank(k,2)+1.72*rank(k,3)
+.745*rank(k,4)+16.3*rank(k,5);
        sumrankj(k,4)=.085;
    end
    sumrankj(k,2)=1113.61;
    sumrankj(k,3)=(sumrankj(k,1)/50)*(159.17-156.62)+156.62;
end

graphrank(10,1)=max(sumrankj(:,3));
graphrank(10,2)=min(sumrankj(:,3));

%Arrangement of top of ice values for plot
for k=1:4
    if graphrank(10,1)==sumrankj(k,3)
        graphrank(10,3)=sumrankj(k,4);
    end

    if graphrank(10,2)==sumrankj(k,3)
        graphrank(10,4)=sumrankj(k,4);
    end
end

for d=1:6
    gsa(d,1)=graphrank(d,1);
    gsa(d,2)=graphrank(d,2);
    gsa(d,3)=graphrank(d,3);
    gsa(d,4)=graphrank(d,4);
end

for d=8:10
    gsa(d-1,1)=graphrank(d,1);
    gsa(d-1,2)=graphrank(d,2);
    gsa(d-1,3)=graphrank(d,3);
    gsa(d-1,4)=graphrank(d,4);
end

bedg= [1108.3 156.09; 1109 155.93; 1109.5 155.63; 1109.98 155.06; 1111
153.58; 1111.55 152.78; 1112.36 150.84; 1113.22 151.78; 1113.61 151.46];

```

```

%Plot of top of ice values
figure;
errorbar (bedg(:,1),gsa(:,1),gsa(:,3)+.242,'--k');
hold on
%scatter(WL1992(:,1),WL1992(:,2),'k');
plot (bed(:,1),bed(:,2),'k');
%errorbar(IJPG1992(:,1),IJPG1992(:,2),IJPG1992(:,4),'LineStyle','-.',
'LineWidth',1,'Color',[0.5 0.5 0.5]);
errorbar(IJPG2007(:,1),IJPG2007(:,2),IJPG2007(:,4),'LineStyle','-.',
'LineWidth',1,'Color',[0.5 0.5 0.5]);
plot(Landmarks(1:36,1),Landmarks(1:36,2),'k')
plot(Landmarks(1:64,5),Landmarks(1:64,6),'k')
plot(Landmarks(1:65,7),Landmarks(1:65,8),'k')
plot(Landmarks(1:38,3),Landmarks(1:38,4),'k')
plot(Landmarks(1:65,9),Landmarks(1:65,10),'k')
errorbar (bedg(:,1),gsa(:,2),gsa(:,4)+.242,'--k');
ylim([150 169]);
xlim([1108 1114]);
xlabel('Distance (km)','FontWeight','Bold');
ylabel('Elevation (m)','FontWeight','Bold');
legend('Proposed Prediction Tool','Bed','Ice Jam Profile
Generator','Landmarks');

```